Theory of double ionization of a neighboring molecule by interatomic Coulombic decay

Jacqueline Fedyk, Kirill Gokhberg, and Lorenz S. Cederbaum
Theoretische Chemie, Physikalisch-Chemisches Institut, Universität Heidelberg, Im Neuenheimer Feld 229, D-69120 Heidelberg, Germany

(Received 16 November 2020; accepted 21 January 2021; published 12 February 2021)

Several known processes, such as single-photon double ionization and double Auger decay, result in correlated emission of two electrons from an atom or molecule. The ratio of double to single ionization in these processes usually amounts only to several percent. Recently, an experiment was reported in helium droplets doped with alkali dimers, where double ionization of the dimer after excitation of the helium proceeds via interatomic Coulombic decay and occurs with an efficiency comparable to that of single ionization via the usual interatomic Coulombic decay. Motivated by these experimental results, we investigate here the theory of this double interatomic Coulombic decay (dICD) process. First, we develop an explicit asymptotic formula for the decay width of dICD based on the assumption that the electronically excited system providing the necessary excess energy and its neighbor are spatially well separated. This formula contains only quantities accessible experimentally for the separated entities – the system and its neighbor. Second, we derive a general analytical expression for the decay width of dICD by using many-body perturbation theory. Finally, we investigated the efficiency of dICD for experimentally realizable small atomic and molecular clusters employing the asymptotic formula.

DOI: 10.1103/PhysRevA.103.022816

I. INTRODUCTION

Among the processes which lead to correlated emission of two electrons after absorption of one photon, single-photon double ionization (SPDI) [1–5] and double Auger [6–10] are the best known. In the former, the two electrons escape directly following the photon absorption; in the latter, they escape in the decay of a metastable core-ionized state. This concerted double-electron emission is primarily due to the electron correlation in the final ionized state [2]. It is common to describe its effect in terms of shake-off and knock-out mechanisms [2,3,11]. In the shake-off mechanism, the first electron is emitted rapidly. The sudden change in the potential is felt by the remaining electrons and their subsequent relaxation leads to the ejection of the second electron. Accordingly, the signature of the shake-off process in the electron kinetic energy spectrum appears as peaks at high (first electron) and low (second electron) electron energies [10,12]. In contrast, the knock-out mechanism can be seen as an impact ionization, whereby the first emitted electron collides inelastically with a bound electron as it exits the collision region, with the result that both electrons are ejected into the continuum. Its signature in the electron spectrum is flatter, although it shows a preference for one slow and one fast electron peak.

In single-photon double ionization, the knock-out dominates at photon energies near the double-ionization threshold [1,11,13], while the shake-off mechanism becomes dominant for high photon energies. Both mechanisms appear also in the double Auger decay, and it has been shown that the knock-out mechanism dominates [7–9]. The ratios of the single-photon double-ionization to single-ionization cross sections usually amount to a few percentage points near the double-ionization threshold [5,11,14–16]. The branching ratios of the double to the normal Auger decay [7,8,13,17,18] are comparable to the typical SPDI to single ionization ratios. For large photon energies over 200 eV, these ratios can reach values up to 80% in some systems [13,19].

In both of these processes, electron emission occurs at the atom or molecule which absorbs the photon. However, a nonlocal process was suggested [20], whereby the absorption of a photon and emission of two electrons occur on different weakly interacting species, specifically a guest atom and a C_{60} cage of an endohedral fullerene. For example, removing a $2p$ electron of Mg in $Mg@C_{60}$ creates an electronically unstable state. As a result, C_{60} can be ionized in an electronic energy transfer between the excited $Mg^+(2p^{-1})$ ion and the carbon cage. For single ionization, this process is known as interatomic Coulombic decay (ICD) [21–25]. However, since the transferred energy in this example is larger than the double-ionization threshold of C_{60}, two electrons can be also emitted into the continuum in a process, which was named double interatomic (intermolecular) Coulombic decay (dICD) [20].

The dICD process is formally related both to the double Auger decay and the single-photon double-ionization processes. As in double Auger decay, a resonance state is present whose decay leads to double-electron emission. In the above example of $Mg@C_{60}$, the magnesium atom is initially ionized forming $Mg^+(2p^{-1})$. In the presence of C_{60}, this ion can transfer its excess energy [by relaxing to $Mg^+(3s^{-1})$] to the fullerene cage and doubly ionize it. ICD involves radiationless energy transfer between the excited species and its neighbor, which at large distances between them can be described as the transfer of a virtual photon [26–29]. Since the absorption of

the virtual photon by the neighbor leads to the emission of two electrons, dICD is related to SPDI. As a result, the discussion of the dICD process can be carried out in terms of the knock-out, shake-off, and ground-state-correlation mechanisms.

The dICD process was recently demonstrated in experiments on He droplets doped with alkali dimers [30]. The droplets were irradiated by XUV photons which led to photoexcitation of He atoms. The energy released in subsequent relaxation of He was transferred to the dimers adsorbed on the droplet's surface which resulted in their ionization. The electron spectra displayed peaks at lower and higher electron energy, which had the characteristic U-shape profile and indicated that two electrons were emitted in concert in the interatomic decay step. Apart from demonstrating the existence of dICD, the experiment showed that its efficiency is comparable to that of ICD, so that the dICD to ICD branching ratio is much larger than the branching ratios commonly seen for the double Auger or SPDI processes.

Recently, resonant dICD in $Li^{2+}He$ was investigated theoretically [31]. Resonant photoexcitation of $Li^{2+}(1s \rightarrow 2p)$ leads to the transfer of its excess energy (91.8 eV) radiationlessly to the neighboring atomic He, which is doubly ionized. dICD was shown to be more efficient than SPDI and for random interatomic orientation, it was found that the averaged angular distribution of resonant dICD qualitatively differs from the one of SPDI.

Motivated by these results of [20,30–32], we investigate in the present work the general theory of the dICD process and put it in relation to the common ICD process. For this purpose, we derive the expression for the decay width of dICD, Γ_{dICD}. As a first step, we develop an asymptotic formula, based on the assumption that the system initially carrying the excess energy and its neighbor, which is doubly ionized by the energy transfer process, are spatially well separated and can be treated as independent entities. Beyond this approximation, we also derive a general analytical expression for the T matrix of the dICD process employing many-body perturbation theory in second order. The numerical evaluation of the resulting expression is rather involved and beyond the scope of the present work. Nevertheless, one can identify in this expression several mechanisms which constitute dICD and explicitly recover the asymptotic expression. Finally, we discuss the dICD width and its ratio to the ICD width for a palette of atomic and molecular systems making explicit use of the derived asymptotic formula.

II. THEORETICAL FRAMEWORK

For simplicity, we consider a system consisting of two species A and B separated by the distance R, whereby A and B can be atoms or molecules. The initial electronic excitation on species A is produced by removing an electron from an inner-valence orbital. If the energy of the excited state is larger than the double-ionization threshold of the combined system, the resulting excited ion can decay via the dICD mechanism, in which relaxation of the initial excitation is accompanied by radiationless energy transfer and simultaneous ejection of two electrons from the outer-valence shell of species B into the continuum (see Fig. 1). Thus, the considered decay

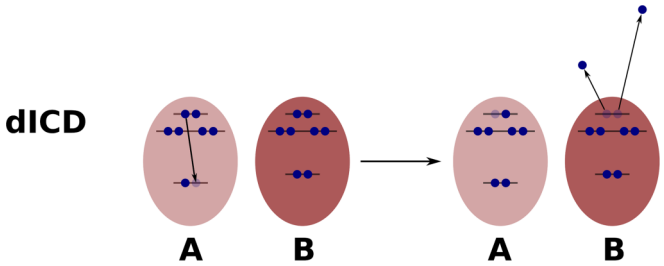

FIG. 1. Simplified scheme of double interatomic (intermolecular) Coulombic decay (dICD), where after the relaxation of the initially electronically excited species A, two electrons of species B are emitted simultaneously.

mechanism reads

$$A^{+*} + B \rightarrow A^{+} + B^{++} + e + e',$$

where e and e' are the two ICD electrons. Inner-valence ionization of neutral species is not a unique mechanism for producing electronically excited states, which might decay in an interatomic process. Electronically excited neutral or multiply ionized atoms or molecules were shown to undergo ICD [21,24,33–41]. However, to keep the presentation simple we will continue the discussion in terms of the inner-valence ionized states. The generalization to other types of excitations is usually straightforward. The efficiency of dICD is determined by its decay rate, and we present below some approaches for its computation.

A. Asymptotic approach

In the following derivation, we assume that the interatomic distance R is fixed. Following the excitation step, the system A-B is found in a decaying electronic state $|\Psi_D\rangle$, which comprises the excited inner-valence ionized species A^{+*} and the neighbor B. This decaying state lies energetically in the double continuum corresponding to the relaxed ion A^+ and a doubly ionized state of B. We denote the energies of the two electrons in the continuum as ε_k and $\varepsilon_{k'}$. The final state of the system can be written as $|\Psi_{E_\gamma,\varepsilon,\varepsilon_{k'}}\rangle$, where E_γ is the energy of the remaining ion (A^+B^{2+}) in the state γ, which is accessible in the decay, and $\varepsilon = \varepsilon_k + \varepsilon_{k'}$. The electronic part of the final state at fixed R is energy-normalized in ε and $\varepsilon_{k'}$, i.e., $\langle\Psi^*_{E_{\gamma'},\varepsilon',\varepsilon'_{k'}}|\Psi_{E_\gamma,\varepsilon,\varepsilon_{k'}}\rangle = \delta_{\gamma\gamma'}\,\delta(\varepsilon-\varepsilon')\delta(\varepsilon_{k'}-\varepsilon'_{k'})$.

The *differential partial decay width* $\Gamma_{E_\gamma}(\varepsilon,\varepsilon_{k'})$ [3,6], which corresponds to the decay of the state $|\Psi_D\rangle$ to the state $|\Psi_{E_\gamma,\varepsilon,\varepsilon_{k'}}\rangle$, is given by the following equation,

$$\Gamma_{E_\gamma}(\varepsilon,\varepsilon_{k'}) = 2\pi\left|\left\langle\Psi_{E_\gamma,\varepsilon,\varepsilon_{k'}}\middle|\hat{H}|\Psi_D\right\rangle\right|^2, \tag{1}$$

where $\hat{H}$ denotes the full electronic Hamiltonian, and neither $|\Psi_D\rangle$ nor $|\Psi_{E_\gamma,\varepsilon,\varepsilon_{k'}}\rangle$ is an eigenstate of $\hat{H}$. By integrating $\Gamma_{E_\gamma}(\varepsilon,\varepsilon_{k'})$ over $\varepsilon_{k'}$, we get an expression for the decay width which corresponds to one specific decay on A accompanied by the emission of two electrons with the combined energy ε from specific orbitals of B. We call this expression *partial decay width for a given channel*,

$$\Gamma_{E_\gamma}(\varepsilon) = \int_0^{\varepsilon} \Gamma_{E_\gamma}(\varepsilon,\varepsilon_{k'})\,d\varepsilon_{k'}. \tag{2}$$

If the interatomic distance R between the two centers A and B is considered in the limit $R \to \infty$, several assumptions become valid, and we will be able to derive an analytical expression for the asymptotic decay width [26–29]. Thanks to the large separation of A and B, the subsystems can be seen as isolated, which allows us to approximate the states of interest as direct products of the states of A and B. The resulting expressions read

$$|\Psi_D\rangle = \left|\Psi_D^{(A)}\right\rangle \left|\Psi_0^{(B)}\right\rangle, \tag{3a}$$

$$\left|\Psi_{E_\gamma,\varepsilon,\varepsilon_{k'}}\right\rangle = \left|\Psi_{E_{\gamma_A}}^{(A)}\right\rangle \left|\Psi_{E_{\gamma_B},\varepsilon,\varepsilon_{k'}}^{(B)}\right\rangle, \tag{3b}$$

where $|\Psi_D^{(A)}\rangle$ represents species A in an inner-valence ionized state, while we assume that $|\Psi_0^{(B)}\rangle$ is the ground state of species B. The double ionization of species B by radiationless energy transfer can then be conceptualized as proceeding via absorbing a single virtual photon emitted in deexcitation of A^{+*}. A final state of the system is a product of the energetically accessible low-lying state of the ion A^+, $|\Psi_{E_{\gamma_A}}^{(A)}\rangle$, and a state $|\Psi_{E_{\gamma_B},\varepsilon,\varepsilon_{k'}}^{(B)}\rangle$ which describes the doubly charged ion of B^{2+} with two emitted electrons in the continuum.

The electronic Hamiltonian can be written as

$$\hat{H} = \hat{H}_A + \hat{H}_B + \hat{W}_{AB} + \hat{V}_{AB}, \tag{4}$$

where $\hat{H}_A$ and $\hat{H}_B$ are the full electronic Hamiltonians of isolated A and B, respectively, $\hat{W}_{AB}$ is the interaction of the electrons of A with the nuclei of B and vice versa, and $\hat{V}_{AB}$ is the Coulomb interaction between the electrons of A and B. The states of the isolated subsystems of A and B are eigenstates of the Hamiltonians $\hat{H}_A$ and $\hat{H}_B$, respectively. The transition from $|\Psi_D\rangle$ to $|\Psi_{E_\gamma,\varepsilon,\varepsilon_{k'}}\rangle$ is effected already in second-order perturbation theory due to the interatomic (intermolecular) two-electron term $\hat{V}_{AB}$, while the coupling of the excited state to the double continuum of the neighbor via the one-particle operator $\hat{W}_{AB}$ occurs in higher orders and can be neglected.

We write the differential partial decay width as

$$\Gamma_{E_\gamma}(\varepsilon, \varepsilon_{k'}) = 2\pi \left|\left\langle \Psi_{E_{\gamma_A}}^{(A)}\right| \left\langle \Psi_{E_{\gamma_B},\varepsilon,\varepsilon_{k'}}^{(B)}\right| \hat{V}_{AB} \left|\Psi_D^{(A)}\right\rangle \left|\Psi_0^{(B)}\right\rangle\right|^2. \tag{5}$$

Before we evaluate the transition amplitude in Eq. (5) in the asymptotic limit, we focus on the Coulomb operator $\hat{V}_{AB}$, which is given as

$$\hat{V}_{AB} = \sum_{i\in A}\sum_{j\in B} \frac{e^2}{\left|\boldsymbol{r}_j^{(B)} - \boldsymbol{r}_i^{(A)}\right|}. \tag{6}$$

The corresponding system is schematically depicted in Fig. 2, where the center of species A is placed at the origin, and the vector $\boldsymbol{R} = R\,\boldsymbol{e}_R$ connects the centers of the species A and B.

The electron coordinates in A and B relative to the origin are $\boldsymbol{r}_i^{(A)}$ and $\boldsymbol{r}_j^{(B)}$, where i enumerates the electrons of A and j enumerates the electrons of B. The vectors $\boldsymbol{r}_i$ and $\boldsymbol{\xi}_j$ are the electron coordinates relative to the centers of A and B, respectively. We assume that in the case of atoms their centers coincide with the nuclei, while for molecules they are located at the respective centers of electronic charge.

At large R, $|\boldsymbol{r}_i^{(A)}| \ll |\boldsymbol{r}_j^{(B)}|$ holds and the Coulomb term can be represented as multipole expansion, whereby only the leading terms are retained. Inserting $\boldsymbol{r}_j^{(B)} = \boldsymbol{R} + \boldsymbol{\xi}_j$ into Eq. (6) (see Fig. 2) and carrying out the multipole expansion in powers of $1/R$, one finds that the first term in Eq. (6) which couples electrons of A and B behaves as $1/R^3$. The Coulomb interaction now reads

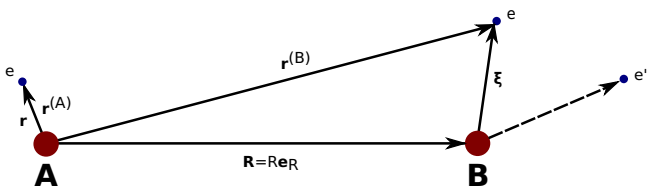

FIG. 2. Schematic configuration of species A and species B with distance R. The coordinates $\boldsymbol{r}^{(A)}$ and $\boldsymbol{r}^{(B)}$ describe the positions of electrons localized on A or B with respect to the species A, while $\mathbf{r}$ and $\boldsymbol{\xi}$ are the corresponding coordinates to A and B, respectively. Electron e receives the energy following the relaxation of A and shares it with e' by correlations.

$$\begin{aligned}\hat{V}_{AB} &= \sum_{i\in A}\sum_{j\in B} \frac{e^2}{|\boldsymbol{R} + (\boldsymbol{\xi}_j - \boldsymbol{r}_i)|} \\ &\approx \frac{e^2}{R^3}\sum_{i\in A}\sum_{j\in B}[\boldsymbol{\xi}_j\boldsymbol{r}_i - 3(\boldsymbol{\xi}_j\boldsymbol{e}_R)(\boldsymbol{r}_i\boldsymbol{e}_R)].\end{aligned} \tag{7}$$

The approximate Coulomb interaction in Eq. (7) can be used for evaluating the dICD transition amplitude

$$\begin{aligned}M_{\mathrm{FI}} &= \left\langle \Psi_{E_{\gamma_A}}^{(A)}\right| \left\langle \Psi_{E_{\gamma_B},\varepsilon,\varepsilon_{k'}}^{(B)}\right| \hat{V}_{AB} \left|\Psi_D^{(A)}\right\rangle \left|\Psi_0^{(B)}\right\rangle \\ &\approx \frac{e^2}{R^3}\sum_{i\in A}\sum_{j\in B}\Big[\left\langle \Psi_{E_{\gamma_A}}^{(A)}\right|\boldsymbol{r}_i\left|\Psi_D^{(A)}\right\rangle \left\langle \Psi_{E_{\gamma_B},\varepsilon,\varepsilon_{k'}}^{(B)}\right|\boldsymbol{\xi}_j\left|\Psi_0^{(B)}\right\rangle \\ &\quad - 3\left\langle \Psi_{E_{\gamma_A}}^{(A)}\right|\boldsymbol{r}_i\boldsymbol{e}_R\left|\Psi_D^{(A)}\right\rangle \left\langle \Psi_{E_{\gamma_B},\varepsilon,\varepsilon_{k'}}^{(B)}\right|\boldsymbol{\xi}_j\boldsymbol{e}_R\left|\Psi_0^{(B)}\right\rangle\Big].\end{aligned} \tag{8}$$

By introducing the dipole operators

$$\hat{\boldsymbol{D}}_A = -\sum_{i\in A} e\,\boldsymbol{r}_i, \tag{9a}$$

$$\hat{\boldsymbol{D}}_B = -\sum_{j\in B} e\,\boldsymbol{\xi}_j, \tag{9b}$$

which act only on the electron coordinates of either A or B, we can write the interaction in a form that emphasizes the dipole-dipole coupling between A and B clearly:

$$M_{\mathrm{FI}} = \frac{1}{R^3}\left[\boldsymbol{D}^{(A)}\boldsymbol{D}^{(B)} - 3(\boldsymbol{e}_R\boldsymbol{D}^{(A)})(\boldsymbol{e}_R\boldsymbol{D}^{(B)})\right], \tag{10}$$

where the transition dipole amplitudes $\boldsymbol{D}^{(A)}$ and $\boldsymbol{D}^{(B)}$ are

$$\boldsymbol{D}^{(A)} = \left\langle \Psi_{E_{\gamma_A}}^{(A)}\right|\hat{\boldsymbol{D}}_A\left|\Psi_D^{(A)}\right\rangle, \tag{11a}$$

$$\boldsymbol{D}^{(B)} = \left\langle \Psi_{E_{\gamma_B},\varepsilon,\varepsilon_{k'}}^{(B)}\right|\hat{\boldsymbol{D}}_B\left|\Psi_0^{(B)}\right\rangle. \tag{11b}$$

Choosing the z axis along the $\boldsymbol{e}_R$, we obtain the following expression for the absolute value squared of the transition amplitude:

$$|M_{\mathrm{FI}}|^2 = \frac{1}{R^6}\left|D_x^{(A)}D_x^{(B)} + D_y^{(A)}D_y^{(B)} - 2\,D_z^{(A)}D_z^{(B)}\right|^2, \tag{12}$$

where D_x, D_y, D_z denote the transition matrix elements belonging to the corresponding component of the dipole operator.

In the following, we want to focus on a diatomic system A-B. Therefore, the states of interest can be written in terms of atomic quantum numbers:

$$|\Psi_D\rangle = |\gamma_A E_A J_A M_A\rangle\,|\gamma_B E_B J_B M_B\rangle, \tag{13a}$$

$$\left|\Psi_{E_\gamma \varepsilon \varepsilon_{k'}}\right\rangle = |\gamma'_A E'_A J'_A M'_A\rangle\,|\gamma'_B E'_B J'_B M'_B\rangle, \tag{13b}$$

where E is the energy of the respective atomic state, J is the total angular momentum, M is its projection, and γ denotes all other quantum numbers. Averaging over the projections of the total angular momentum of A and B in the initial state, M_A and M_B, and summing over the final states, M'_A and M'_B, gives [42,43]

$$\begin{aligned}\overline{|M_{\mathrm{FI}}|^2} &= \frac{1}{2J_A+1}\frac{1}{2J_B+1}\sum_{M_A M'_A}\sum_{M_B M'_B}|M_{\mathrm{FI}}|^2 \\ &= \frac{1}{2J_A+1}\frac{1}{2J_B+1}\frac{2}{3R^6}|(\gamma'_A E'_A J'_A||\hat{\boldsymbol{D}}_A||\gamma_A E_A J_A) \\ &\quad\times(\gamma'_B E'_B J'_B||\hat{\boldsymbol{D}}_B||\gamma_B E_B J_B)|^2,\end{aligned} \tag{14}$$

where $(\gamma' E' J'||\hat{\boldsymbol{D}}||\gamma E J)$ stands for the reduced matrix element [42]. In our case, we assume atom B initially in its nondegenerate ground state with $J_B = 0$; thus $\frac{1}{2J_B+1}$ reduces to 1. Finally, the differential partial decay width averaged over the projection of the angular momentum becomes

$$\begin{aligned}\Gamma_{E_\beta}(\varepsilon,\varepsilon_{k'}) &= \frac{4\pi}{3R^6}\frac{1}{2J_A+1}|(\gamma'_A E'_A J'_A||\hat{\boldsymbol{D}}_A||\gamma_A E_A J_A) \\ &\quad\times(\gamma'_B E'_B J'_B||\hat{\boldsymbol{D}}_B||\gamma_B E_B\,0)|^2.\end{aligned} \tag{15}$$

We use Eq. (15) to obtain the partial decay width $\Gamma_{E_\gamma}(\varepsilon)$ [see Eq. (2)]. By summing the latter over all final states, we obtain the total decay width of dICD,

$$\begin{aligned}\Gamma_{\mathrm{dICD}} &= \frac{4\pi}{3R^6}\sum_{F_A F_B}\int_0^{\varepsilon} d\varepsilon_{k'}\,\frac{1}{2J_A+1}\,|(\gamma'_A E'_A J'_A||\hat{\boldsymbol{D}}_{\boldsymbol{A}}||\gamma_A E_A J_A) \\ &\quad\times(\gamma'_B E'_B J'_B||\hat{\boldsymbol{D}}_{\boldsymbol{B}}||\gamma_B E_B\,0)|^2,\end{aligned} \tag{16}$$

whereby F_A (F_B) enumerates the energetically accessible final states of A (B). In the special case where there is only one suitable transition on A we can express the *partial decay width* $\Gamma_{\mathrm{dICD}}(\omega)$ through experimentally measurable quantities of the isolated subsystems A and B. To do that we write for the radiative decay rate on atom A [42]

$$w_A = \frac{4\omega^3}{3\hbar c^3}\frac{1}{2J_A+1}|(\gamma'_A E'_A J'_A||\hat{\boldsymbol{D}}_A||\gamma_A E_A J_A)|^2, \tag{17}$$

where the transition energy $\hbar\omega$ is the energy of the virtual photon:

$$\hbar\omega = E'_A - E_A = E'_B - E_B. \tag{18}$$

The radiative lifetime which corresponds to the transition $(\gamma_A E_A J_A) \to (\gamma'_A E'_A J'_A)$ on A reads

$$\tau_A = \frac{1}{w_A}. \tag{19}$$

Furthermore, the transition moment $|(\gamma'_B E'_B J'_B||\hat{\boldsymbol{D}}_B||\gamma_B E_B J_B)|^2$ is replaced by the *single-differential one-photon double-ionization cross section* of atom B, $\frac{d\sigma_B^{++}(\omega)}{d\varepsilon_{k'}}$, in the length gauge with photons of energy $\hbar\omega$ [2–4],

$$\frac{d\sigma_B^{++}(\omega)}{d\varepsilon_{k'}} = \frac{4\pi^2}{3}\frac{\omega}{c}\sum_{F_B}|(\gamma'_B E'_B J'_B||\hat{\boldsymbol{D}}_B||\gamma_B E_B J_B)|^2, \tag{20}$$

where F_B denotes all energetically possible final states on B and $|\Psi_0^B\rangle$ is the nondegenerate ground state of atom B. The resulting formula for the partial decay width $\Gamma_{\mathrm{dICD}}(\omega)$ of dICD in a system of two atoms defined by measurable quantities for one specific virtual photon energy $\hbar\omega$ finally reads

$$\Gamma_{\mathrm{dICD}}(\omega) = \frac{3\hbar}{4\pi}\left(\frac{c}{\omega}\right)^4\frac{\tau_A^{-1}\sigma_B^{++}(\omega)}{R^6}. \tag{21}$$

Note that the partial decay width $\Gamma_{\mathrm{dICD}}(\omega)$ takes into account different transitions on species B for one specific virtual photon energy, while the partial decay width for a given channel $\Gamma_{E_\gamma}(\varepsilon)$ considers for a given decay on A only one transition on B.

In the asymptotic derivation of the partial decay width, the dipole operators appear naturally in the length gauge, since they arise through the expansion of the Coulomb interaction. Therefore, whenever *ab initio* radiative lifetimes and single-photon double-ionization cross sections are used in Eq. (21), the length gauge should be preferred if the respective transition moments depend on the gauge chosen.

Furthermore, Eq. (21) is not only valid for atomic systems. It is also valid for systems which consist of a decaying atomic species and a molecular species as neighbor if we average over the orientation of the molecule in space [44,45].

B. Many-body perturbation theory approach

In the following, we assume that the decay occurs in a weakly bound cluster A-B, where the characteristic values of R are a few angstroms, and where A and B mostly retain the character of isolated species. In contrast to the derivation of the ICD width, we have to use time-independent many-body perturbation theory to obtain an expression for the decay width Γ_{dICD}. The electronic Hamiltonian is divided into an unperturbed Hamiltonian $\hat{H}_0$ and an interaction Hamiltonian $\hat{H}_I$, which describes the perturbation:

$$\hat{H} = \hat{H}_0 + \hat{H}_I. \tag{22}$$

We select $\hat{H}_0$ as the Hartree-Fock (HF) Hamiltonian and $\hat{H}_I = \hat{V} - \hat{v}^{HF}$ is the interaction Hamiltonian, which contains the Coulomb operator $\hat{V}$ and the average Hartree-Fock potential $\hat{v}^{HF}$. The Hartree-Fock Hamiltonian is given as $\hat{H}_0 = \sum_i \hat{f}(\boldsymbol{r}_i)$, where $\hat{f}$ stands for a one-electron Fock operator and the sum runs over all electrons in the system. The eigenfunctions φ_n and eigenvalues ε_n of the Fock operator are the spin orbitals and the orbital energies.

In the following, we consider N-electron systems with a closed-shell electronic ground state. The decaying state is produced by removing an inner-valence electron, while the final states consist of the triply ionized system with two electrons in the continuum. To describe these states using the perturbation

theory one needs one-hole (1h), one-particle-two-hole (1p2h), and two-particle-three-hole (2p3h) unperturbed states. They are constructed by acting with the physical excitation operators on the HF ground state $|\Phi_0\rangle$:

$$|\Phi_i\rangle = c_i|\Phi_0\rangle, \tag{23a}$$

$$\left|\Phi_{ij}^{a}\right\rangle = c_a^\dagger c_i c_j|\Phi_0\rangle, \tag{23b}$$

$$\left|\Phi_{ijk}^{ab}\right\rangle = c_a^\dagger c_b^\dagger c_i c_j c_k|\Phi_0\rangle, \tag{23c}$$

where c_n and $c_n^\dagger$ are annihilation and creation operators for an electron in the orbital φ_n. Thereby, the indices a and b enumerate the particle orbitals and i, j, and k the hole orbitals. Note that the indices refer to spin orbitals.

The unperturbed states are eigenstates of the unperturbed Hamiltonian $\hat{H}_0$, according to

$$\hat{H}_0\,|\Phi_i\rangle = \left(E_0^{(0)} - \varepsilon_i\right)|\Phi_i\rangle = E_i^{(0)}|\Phi_i\rangle, \tag{24a}$$

$$\hat{H}_0\left|\Phi_{ij}^{a}\right\rangle = \left(E_0^{(0)} + \varepsilon_a - \varepsilon_i - \varepsilon_j\right)\left|\Phi_{ij}^{a}\right\rangle = E_{aij}^{(0)}\left|\Phi_{ij}^{a}\right\rangle, \tag{24b}$$

$$\begin{aligned}\hat{H}_0\left|\Phi_{ijk}^{ab}\right\rangle &= \left(E_0^{(0)} + \varepsilon_a + \varepsilon_b - \varepsilon_i - \varepsilon_j - \varepsilon_k\right)\left|\Phi_{ijk}^{ab}\right\rangle \\ &= E_{abijk}^{(0)}\left|\Phi_{ijk}^{ab}\right\rangle,\end{aligned} \tag{24c}$$

where $E_0^{(0)}$ is the zeroth-order energy of the ground state: $\hat{H}_0\,|\Phi_0\rangle = E_0^{(0)}\,|\Phi_0\rangle$.

As before, we derive the expression for the dICD width for a cluster consisting of two weakly bound components A and B, which we assume initially to be in their closed-shell ground state. Because the bonding is weak for the R of interest, the hole orbitals are just weakly perturbed orbitals of isolated A and B. Therefore, we will retain the indices A and B in denoting the orbitals, to indicate that they are mostly localized on the respective species. The decaying state has a hole in an inner-valence orbital $iv_A \equiv iv_A\eta$ ($\eta = \pm 1/2$ is the spin projection). In the final state there are three holes which occupy the outer-valence orbitals $ov_A \equiv ov_A\lambda$, $ov_B \equiv ov_B\mu$, and $ov_B' \equiv ov_B'\sigma$, while the two particles occupy the continuum orbitals $\varepsilon_k \equiv \varepsilon_k\delta$ and $\varepsilon_{k'} \equiv \varepsilon_{k'}\nu$. We denote the initial state as $|\Psi_{iv_A}\rangle$ and the final state as $|\Psi_{\varepsilon_k\varepsilon_{k'}ov_Aov_Bov_B'}\rangle$, where the spin indices are suppressed for clarity. The total spin of the decaying state is $S = 1/2$, and it is conserved in the decay since $\hat{H}_I$ is spin-free.

Since the transition between the unperturbed decaying and the final states is forbidden in first order, to obtain the dICD transition amplitude we expand them in perturbation theory,

$$\begin{aligned}\left|\Psi_{iv_A}\right\rangle &\approx \left|\Phi_{iv_A}\right\rangle + \frac{\hat{Q}_D}{E_{iv_A}^{(0)} - \hat{H}_0}\hat{H}_I\,|\Phi_{iv_A}\rangle \\ &= \left|\Psi_{iv_A}^{(0)}\right\rangle + \left|\Psi_{iv_A}^{(1)}\right\rangle,\end{aligned} \tag{25a}$$

$$\begin{aligned}\left|\Psi_{\varepsilon_k\varepsilon_{k'}ov_Aov_Bov_B'}\right\rangle &\approx \left|\Phi_{ov_Aov_Bov_B'}^{\varepsilon_k\varepsilon_{k'}}\right\rangle + \frac{\hat{Q}_F}{E_{\varepsilon_k\varepsilon_{k'}ov_Aov_Bov_B'}^{(0)} - \hat{H}_0} \\ &\quad\times \hat{H}_I\left|\Phi_{ov_Aov_Bov_B'}^{\varepsilon_k\varepsilon_{k'}}\right\rangle \\ &= \left|\Psi_{\varepsilon_k\varepsilon_{k'}ov_Aov_Bov_B'}^{(0)}\right\rangle + \left|\Psi_{\varepsilon_k\varepsilon_{k'}ov_Aov_Bov_B'}^{(1)}\right\rangle,\end{aligned} \tag{25b}$$

where $\hat{Q}_D$ and $\hat{Q}_F$ are projectors in the configuration space. The transition amplitude between the initial 1h state $|\Psi_{iv_A}\rangle$ and the final 2p3h state $|\Psi_{\varepsilon_k\varepsilon_{k'}ov_Aov_Bov_B'}\rangle$ becomes

$$\begin{aligned}T_{\varepsilon_k\varepsilon_{k'}ov_Aov_Bov_B':iv_A}^{(2)} &= \left\langle\Phi_{ov_Aov_Bov_B'}^{\varepsilon_k\varepsilon_{k'}}|\hat{H}_I|\Psi_{iv_A}^{(1)}\right\rangle \\ &\quad + \left\langle\Psi_{\varepsilon_k\varepsilon_{k'}ov_Aov_Bov_B'}^{(1)}|\hat{H}_I|\Phi_{iv_A}\right\rangle.\end{aligned} \tag{26}$$

To derive explicit expressions for the transition amplitude we should first construct the projectors $\hat{Q}_D$ and $\hat{Q}_F$. They are of the form $\hat{Q} = \mathbb{1} - \sum_N |\Phi_N\rangle\langle\Phi_N|$, where the sum runs over a subspace of configurations which we select in a special way. First-order corrections are usually defined as orthogonal to the respective unperturbed state [46]. The operators $\hat{Q}_D$ and $\hat{Q}_F$ ensure this orthogonality. We first note that $\hat{Q}_D$ must not include $|\Phi_{iv_A}\rangle\langle\Phi_{iv_A}|$ and $\hat{Q}_F$ must not include $|\Phi_{ov_Aov_Bov_B'}^{\varepsilon_k\varepsilon_{k'}}\rangle\langle\Phi_{ov_Aov_Bov_B'}^{\varepsilon_k\varepsilon_{k'}}|$; otherwise the respective first-order corrections in Eqs. (25a) and (25b) diverge. We also impose the condition that the decaying and the final states are orthogonal [47], in our case through second order in perturbation theory (for full details see Appendix A). The states as defined above are already orthogonal through first order. To ensure orthogonality in second order we first determine a set of virtual states $\{|\Phi_K\rangle\}$ which couple the $|\Phi_{iv_A}\rangle$ and $|\Phi_{ov_Aov_Bov_B'}^{\varepsilon_k\varepsilon_{k'}}\rangle$ in second order. The configurations in this set cannot be simultaneously present in $\hat{Q}_D$ and $\hat{Q}_F$. Therefore, one divides them into two disjoint subsets, such that each subset enters only one projector. As we discuss in Appendix A, division into subsets is not unique, but leads to the same expression of the transition amplitude. In addition one should remove $|\Phi_{ov_Aov_Bov_B'}^{\varepsilon_k\varepsilon_{k'}}\rangle\langle\Phi_{ov_Aov_Bov_B'}^{\varepsilon_k\varepsilon_{k'}}|$ and $|\Phi_{iv_A}\rangle\langle\Phi_{iv_A}|$ from $\hat{Q}_D$ and $\hat{Q}_F$, respectively.

We would like to remark that if orthogonality is not enforced the factor 2 appears in the transition amplitude, since the same contributions come from the expansion of both the initial and final states. The procedure outlined above and in Appendix A leads to the results in conformance with the perturbative expansion of the SPDI and the double Auger amplitudes [2,3,6].

The resulting expression for the transition amplitude $T_{\varepsilon_k\varepsilon_{k'}ov_Aov_Bov_B':iv_A}^{(2)}$ consists of eighteen terms, which can be interpreted in terms of known physical processes. The complete list of the terms and the details of their derivation can be found in Appendix A. In the following, we discuss the structure and the physical meaning of four characteristic terms. We begin with the term which arises when the coupling proceeds via the unperturbed virtual state $\sum_{p_B}|\Phi_{ov_Aov_Bp_B}^{p_B}\rangle\langle\Phi_{ov_Aov_Bp_B}^{p_B}|$ (see Table III, combination 1, in Appendix A). The sum $\sum_{p_B}$ runs over all particle orbitals of B including bound and continuum states. The term reads

$$+\sum_{p_B}\frac{V_{\varepsilon_k\varepsilon_{k'}[ov_B'p_B]}}{\left(\varepsilon_k + \varepsilon_{k'} - \varepsilon_{ov_B'} - \varepsilon_{p_B} + i0^+\right)}V_{p_Biv_Aov_Bov_A}. \tag{27}$$

After the electron transition from the outer-valence orbital ov_A to the inner valence orbital iv_A, an electron of B is ejected from the outer-valence orbital ov_B. The emitted electron p_B interacts with another bound electron of B in the outer-valence orbital ov_B' knocking it out, which leads to two electrons ε_k and ε_k' in the continuum. This process encoded in the amplitude in Eq. (27) [see Fig. 3(a)] can be interpreted as an ICD step followed by knock-out ionization of B. The energy denominator has a singularity for the limiting case, if

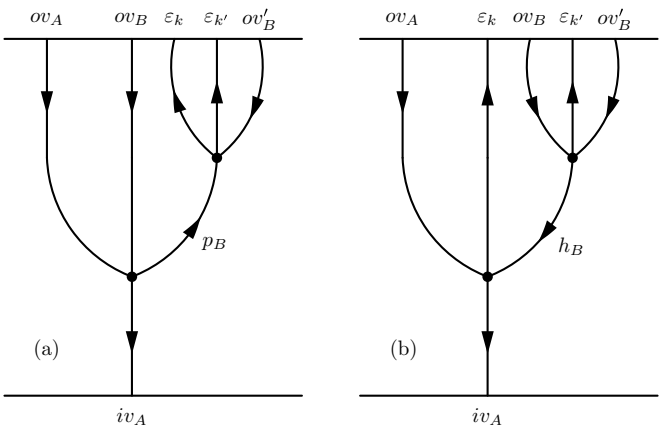

FIG. 3. Diagrammatic representation of the dICD transition amplitudes which correspond to the knock-out (a) and the shake-off (b) mechanisms. The horizontal lines represent the initial and the final states. The dots denote the interaction. The arrows pointed downward denote occupied (hole) orbitals, while the arrows pointed upward denote unoccupied (particles) orbitals.

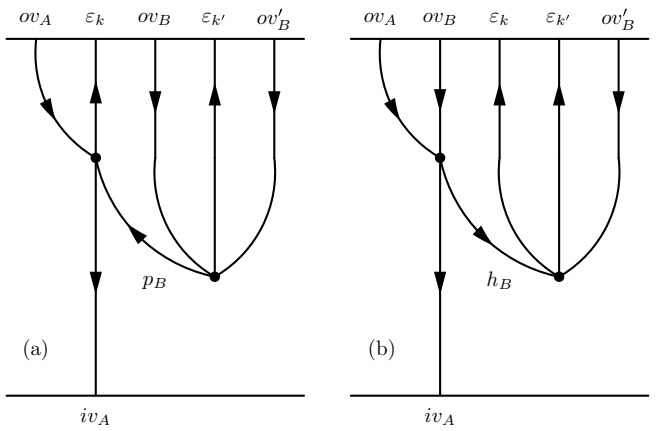

FIG. 4. Diagrammatic representation of the dICD transition amplitudes which correspond to ground-state correlations: coupling via particle orbital p_B (a) and coupling via hole orbital h_B (b). The horizontal lines represent the initial and the final states. The dots denote the interaction. The arrows pointed downward denote occupied (hole) orbitals and the arrows pointed upward denote unoccupied (particles) orbitals.

one of the emitted electrons takes the whole excess energy: $\varepsilon_{p_B} = \varepsilon_k + \varepsilon_{k'} - \varepsilon_{ov'_B}$. Therefore, an infinitesimal imaginary part $+i0^+$ has to be added to the energy denominator. The process is analogous to that describing the knock-out mechanism in double Auger decay or SPDI, where it is the dominant mechanism for photon energies near the double-ionization threshold [2–10].

Next, we consider the term [see Fig. 3(b)] obtained by inserting the unperturbed virtual state $\sum_{h_B} |\Phi^{\varepsilon_k}_{ov_A h_B}\rangle \langle \Phi^{\varepsilon_k}_{ov_A h_B}|$ into the dICD transition amplitude in Eq. (26) (see Table III, combination 1, in Appendix A). The result reads

$$-\sum_{h_B} V_{iv_A \varepsilon_k ov_A h_B} \frac{V_{h_B \varepsilon_{k'} [ov_B ov'_B]}}{\left(\varepsilon_{h_B} + \varepsilon_{k'} - \varepsilon_{ov_B} - \varepsilon_{ov'_B}\right)}, \tag{28}$$

where the summation runs over all hole orbitals on B. The first matrix element is the ICD amplitude, which corresponds to the relaxation of the initial vacancy on A and the first ionization of B. The second matrix element describes the relaxation of B accompanied by the emission of the second electron. In other words, following the energy transfer in ICD the electron of B is ejected from h_B to the continuum with the energy ε_k. Because of this sudden ionization, the potential on B changes rapidly, and the orbital relaxation leads to the emission of another electron from ov'_B, which has the electron energy $\varepsilon_{k'}$; see Fig. 3(b). This mechanism is analogous to shake-off processes, which appear in double Auger and SPDI.

In the last two examples, we focus on the unperturbed virtual 2p3h states, $\sum_{p_1 p_2 h_1 h_2 h_3} |\Phi^{p_1 p_2}_{h_1 h_2 h_3}\rangle \langle \Phi^{p_1 p_2}_{h_1 h_2 h_3}|$. The presented terms arise by inserting the unperturbed states $|\Phi^{p_B \varepsilon_{k'}}_{ov_B ov'_B iv_A}\rangle$ and $|\Phi^{\varepsilon_k \varepsilon_{k'}}_{ov'_B h_B iv_A}\rangle$ (see Table IV, configurations 5 and 3, in Appendix A) into the dICD transition amplitude [see Eq. (26)]:

$$-\sum_{p_B} V_{iv_A \varepsilon_k ov_A p_B} \frac{V_{p_B \varepsilon_{k'} [ov_B ov'_B]}}{\left(\varepsilon_{p_B} + \varepsilon_{k'} - \varepsilon_{ov_B} - \varepsilon_{ov'_B}\right)}, \tag{29}$$

$$+\sum_{h_B} \frac{V_{\varepsilon_k \varepsilon_{k'} [ov'_B h_B]}}{\left(\varepsilon_k + \varepsilon_{k'} - \varepsilon_{ov'_B} - \varepsilon_{h_B}\right)} V_{h_B iv_A ov_B ov_A}. \tag{30}$$

Both terms include the electron transition from ov_A to iv_A and the direct double ionization of B, where the coupling between the two species proceeds in Eq. (29) via particle and in Eq. (30) via hole orbitals. These two mechanisms can be understood as stemming from the ground-state correlations of the two species participating in dICD (see Fig. 4). These double-ionization pathways due to ground-state correlations are known for SPDI, where they arise from the perturbative expansion of the ground state of an atom or a molecule being ionized. Similar mechanisms also appear in double Auger decay when unperturbed 2p3h states are used in the first-order expansion of the core-hole state.

The transition amplitude $T^{(2)}_{\varepsilon_k \varepsilon_{k'} ov_A ov_B ov'_B; iv_A}$ (see Appendix A) refers to a specific set of spin orbitals. To construct the differential partial decay width $\Gamma_{ov_A ov_B ov'_B}(\varepsilon, \varepsilon_{k'})$ for a state-to-state transition according to Eq. (15), one has to deal with both spin and spatial degeneracies of the involving orbitals. This means that for a final state characterized by spatial orbitals ov_A, ov_B, and ov'_B one has to average over initial-state and to sum over final-state degeneracies [42]. In the case of an atomic system the orbitals iv_A, ov_A, ov_B, and ov'_B are described by orbital angular momenta l and the respective degeneracies are given by the magnetic quantum numbers m_l. Consequently, the absolute value squared reads

$$\overline{\left|T^{(2)}_{\varepsilon_k \varepsilon_{k'} ov_A ov_B ov'_B; iv_A}\right|^2} = \frac{1}{2\,l_{iv_A}+1} \frac{1}{2\,s_{iv_A}+1} \times \sum_{\substack{m_{l_{iv_A}} m_{l_{ov_A}} \\ m_{l_{ov_B}} m_{l_{ov'_B}}}} \sum_{\eta\lambda\delta\nu\mu\sigma} \left|T^{(2)}_{\varepsilon_k \varepsilon_{k'} ov_A ov_B ov'_B; iv_A}\right|^2. \tag{31}$$

It follows for the differential partial decay width according to Eq. (15):

$$\Gamma_{ov_A ov_B ov'_B}(\varepsilon, \varepsilon_{k'}) = 2\pi \overline{\left|T^{(2)}_{\varepsilon_k \varepsilon_{k'} ov_A ov_B ov'_B; iv_A}\right|^2}. \tag{32}$$

By integrating the differential partial decay width over the energy of one of the emitted electrons and by summing over different degenerate final states of B we obtain the partial decay width which corresponds to some virtual photon energy $\hbar\omega$ [see also Eq. (21)]:

$$\Gamma_{\mathrm{dICD}}(\omega) = \sum_{ov_B ov'_B} \int_0^{\varepsilon} \Gamma_{ov_A ov_B ov'_B}(\varepsilon, \varepsilon_{k'})\, d\varepsilon_{k'}. \tag{33}$$

For the total decay width of dICD, the summation over the spin orbital ov_A is added. The sum $\sum_{ov_A ov_B ov'_B}$ includes different relaxation pathways of A and thus different virtual photon energies. Consequently, it contains all energetically possible transitions on B for the given virtual photon energies. The total decay width of dICD reads

$$\Gamma_{\mathrm{dICD}} = \sum_{ov_A ov_B ov'_B} \int_0^{\varepsilon} \Gamma_{ov_A ov_B ov'_B}(\varepsilon, \varepsilon_{k'})\, d\varepsilon_{k'}. \tag{34}$$

Once the values of the two-electron integrals and the orbital energies are known, the various widths can be computed numerically.

C. Derivation of the asymptotic expression from the perturbatively derived transition amplitude

In this subsection, we show that the expression Γ_{dICD} in Eq. (34) correctly reduces to Eq. (21) for $R \to \infty$. The total Coulomb operator $\hat{V}$ is rewritten as

$$\hat{V} = \hat{V}_A + \hat{V}_B + \hat{V}_{AB}. \tag{35}$$

$\hat{V}_A$ and $\hat{V}_B$ are the electron repulsion operators of A and B, which are responsible for local processes, while $\hat{V}_{AB}$ represents the interaction between the electrons of A and B. The amplitudes, which involve electron transfer, decay exponentially with R and can be neglected [48]. Furthermore, the interaction Coulomb operator $\hat{V}_{AB}$ is expanded [see Eq. (7)]. The effect of these two approximations is to reduce the number of terms in the transition amplitude from eighteen to eight, see Appendix B, which represents the four different mechanisms: knock-out (KO), shake-off (SO), and the two types of ground-state correlations (GSC_p and GSC_h) as described above.

After the multipole expansion of the interaction Coulomb operator $\hat{V}_{AB}$ the Coulomb integrals of the surviving eight terms of the form $V_{p_B i v_A h_B ov_A}$ read

$$V_{p_B i v_A h_B ov_A} \approx \frac{1}{R^3}\big[\langle\varphi_{iv_A}|\hat{\boldsymbol{d}}_A|\varphi_{ov_A}\rangle\langle\varphi_{p_B}|\hat{\boldsymbol{d}}_B|\varphi_{h_B}\rangle - 3\langle\varphi_{iv_A}|\hat{\boldsymbol{d}}_A\boldsymbol{e}_{\boldsymbol{R}}|\varphi_{ov_A}\rangle\langle\varphi_{p_B}|\hat{\boldsymbol{d}}_B\boldsymbol{e}_{\boldsymbol{R}}|\varphi_{h_B}\rangle\big]. \tag{36}$$

Inserting this expansion into the surviving eight terms of the transition amplitude [see Eq. (B1) in Appendix B] and averaging its absolute value squared over the degeneracies allows us to represent the width via quantities related to isolated A and B. The dICD transition amplitude becomes a product of the dipole transition amplitude on A, $\langle\varphi_{iv_A}|\hat{\boldsymbol{d}}_A|\varphi_{ov_A}\rangle$, and of the double-ionization amplitude of B, $\boldsymbol{T}(KO) + \boldsymbol{T}(SO) + \boldsymbol{T}(GSC_p) + \boldsymbol{T}(GSC_h)$. For details of the derivation, see Appendix B. The total decay width of dICD Γ_{dICD} [see Eq. (34)] expressed by the various individual transition amplitudes reads

$$\Gamma_{\mathrm{dICD}} = 2\pi \frac{2}{3R^6} \sum_{ov_A} \overline{\left|\langle\varphi_{iv_A}|\hat{\boldsymbol{d}}_A|\varphi_{ov_A}\rangle\right|^2} \sum_{ov_B ov'_B} \int_0^{\varepsilon} d\varepsilon_{k'} \times \overline{\left|\boldsymbol{T}(KO) + \boldsymbol{T}(SO) + \boldsymbol{T}(GSC_p) + \boldsymbol{T}(GSC_h)\right|^2}, \tag{37}$$

where the overlines denote that the absolute values squared of the corresponding transition amplitudes are averaged over degeneracies. $T(KO)$ and $T(SO)$ are respectively the knock-out and the shake-off amplitudes, while $T(GSC_p)$ and $T(GSC_h)$ appear due to the ground-state correlations. The sum of these transition amplitudes equals the total amplitude of the SPDI cross section [2,3]. Employing Eq. (20), we rewrite the single-differential SPDI cross section to be in our nomenclature [2–4]:

$$\frac{d\sigma_B^{++}(\omega)}{d\varepsilon_{k'}} = \frac{4\pi^2}{3}\frac{\omega}{c} \sum_{ov_B ov'_B} \overline{\left|T(KO) + T(SO) + T(GSC_p) + T(GSC_h)\right|^2}. \tag{38}$$

The explicit SPDI amplitudes in our nomenclature can be found in Appendix C.

As in Sec. II A, the lifetime τ_A [see Eq. (19)] and the single-differential single-photon double-ionization cross section $\frac{d\sigma_B^{++}(\omega)}{d\varepsilon_{k'}}$ [see Eq. (38)] can be identified in the expression for the dICD rate [see Eq. (37)]. As $\frac{d\sigma_B^{++}(\omega)}{d\varepsilon_{k'}}$ takes only one virtual photon energy into account, one can consider a single relaxation pathway of A and finally arrive at the asymptotic partial decay width

$$\Gamma_{\mathrm{dICD}}(\omega) = \frac{3\hbar}{4\pi}\left(\frac{c}{\omega}\right)^4 \frac{\tau_A^{-1}\sigma_B^{++}(\omega)}{R^6}, \tag{39}$$

which coincides with the expression for the dICD rate derived above directly from the golden rule at large R [see Eq. (21) in Sec. II A].

III. APPLICATIONS

In this section, we apply the asymptotic expression in Eq. (21) to investigate dICD and compare its efficiency to that of ICD and other decay processes. For ICD it has been shown that at shorter distances R, where the respective asymptotic expression loses its validity, the ICD rates obtained by this expression can be much smaller than the precise rates due to orbital overlap and can be seen as a lower bound to the latter [26]. Since two electrons are emitted in dICD and thus at least two orbitals of the neighbor are involved in the process, one can expect that orbital overlap may have an even larger impact on the rate than found for ICD. Thus, at smaller R, the rates obtained by the asymptotic expression are also to be seen as lower bounds to the precise, but yet unknown, rates.

TABLE I. ICD and dICD rates for endohedral fullerenes. For each system the first row shows the data of the guest atom and the second row the data of C_{60} at the respective virtual photon energy. The third row reports the desired rates for the respective endohedral fullerene. Note that the dICD channel is not open for Ne@C_{60} due to the Coulomb repulsion in the final state. E_{vp} is the excess energy (virtual photon energy), w_A is the radiative rate, τ_A is the respective radiative lifetime of the isolated guest atom, DIP is the double-ionization potential of C_{60}, σ_B^{++} and σ_B^{+} are the double- and single-ionization cross sections at the corresponding virtual photon energies, $\Gamma_{\rm ICD}$ and $\Gamma_{\rm dICD}$ are the ICD and dICD decay rates, and $\tau_{\rm ICD}$ and $\tau_{\rm dICD}$ are the resulting lifetimes due to the process indicated.

Ne@C_{60}	$R = 3.4$ Å [49]		
$Ne^+(2s^1 2p^6 \rightarrow 2s^2 2p^5)$	$E_{vp} = 26.9$ eV [52]	$w_A = 5.5 \times 10^9$ 1/s [52]	$\tau_A = 1.9 \times 10^{-10}$ s
C_{60} [53–55]	DIP = 19 eV		$\sigma_B^{+} = 5.7 \times 10^2$ Mb
ICD	$\Gamma_{\rm ICD} = 9.3 \times 10^{-2}$ eV	$\Gamma_{\rm ICD} = 1.4 \times 10^{14}$ 1/s	$\tau_{\rm ICD} = 7.1 \times 10^{-15}$ s
Mg@C_{60}	$R = 3.5$ Å [56]		
$Mg^+(2p^5 3s^2 \rightarrow 2p^6 3s)$	$E_{vp} = 50.2$ eV [52]	$w_A = 4.7 \times 10^9$ 1/s	$\tau_A = 2.1 \times 10^{-10}$ s [57]
C_{60} [53–55]	DIP=19 eV	$\sigma_B^{++} = 2.2 \times 10^1$ Mb	$\sigma_B^{+} = 8.9 \times 10^1$ Mb
ICD	$\Gamma_{\rm ICD} = 8.6 \times 10^{-4}$ eV	$\Gamma_{\rm ICD} = 1.3 \times 10^{12}$ 1/s	$\tau_{\rm ICD} = 7.7 \times 10^{-13}$ s
dICD	$\Gamma_{\rm dICD} = 2.1 \times 10^{-4}$ eV	$\Gamma_{\rm dICD} = 3.2 \times 10^{11}$ 1/s	$\tau_{\rm dICD} = 3.1 \times 10^{-12}$ s
He@C_{60}	$R = 3.3$ Å [49]		
$He^*(1s2p \rightarrow 1s^2)$	$E_{vp} = 21.2$ eV [52]	$w_A = 1.8 \times 10^9$ 1/s [52]	$\tau_A = 5.6 \times 10^{-10}$ s
C_{60} [53–55]	DIP= 19 eV	$\sigma_B^{++} = 1.4$ Mb	$\sigma_B^{+} = 1.2 \times 10^3$ Mb
ICD	$\Gamma_{\rm ICD} = 2.0 \times 10^{-1}$ eV	$\Gamma_{\rm ICD} = 2.9 \times 10^{14}$ 1/s	$\tau_{\rm ICD} = 3.5 \times 10^{-15}$ s
dICD	$\Gamma_{\rm dICD} = 2.3 \times 10^{-4}$ eV	$\Gamma_{\rm dICD} = 3.5 \times 10^{11}$ 1/s	$\tau_{\rm dICD} = 2.9 \times 10^{-12}$ s

Following the first observation that dICD is possible in Mg@C_{60} [20], we start the discussion with the fullerene C_{60} as a neighbor. It is well known that C_{60} and other fullerenes accommodate foreign atoms and molecules [49–51]. Here, we shall concentrate on the endohedral fullerenes Ne@C_{60}, Mg@C_{60}, and He@C_{60}.

We start with Ne@C_{60} after $2s$ ionization of Ne. The excess energy (see Table I) is 26.9 eV and, of course, suffices to ionize via ICD the C_{60} cage. However, due to the large Coulomb repulsion of 8.4 eV between Ne^+ and the resulting C_{60}^{++}, dICD is just not possible. Here, the ICD rate has been computed by *ab initio* methods [20] and we use this fact to compare the result with that of the asymptotic expression. The asymptotic expression for the ICD rate reads [26]

$$\Gamma_{\rm ICD} = \frac{3\hbar}{4\pi}\left(\frac{c}{\omega}\right)^4 \frac{\tau_A^{-1}\sigma_B^{+}}{R^6}. \tag{40}$$

As can be seen from Table I, the lifetime of the $Ne^+(2s^{-1})$ ion reduces from the lifetime of the isolated ion of 0.2 ns to only 7 fs due to ICD. The reported *ab initio* value is shorter and amounts to 2 fs [20].

As noted in Ref. [20], the dICD channel is open in Mg@C_{60} after $2p$ ionization of Mg. As indicated in Table I, the excess energy of $Mg^+(2p^{-1})$ is over 50 eV and by far suffices for dICD to take place. To be able to easily compute the ICD and dICD rates, we present in the following the decay width in practical units,

$$\Gamma_{\rm dICD}[\text{eV}] = 2.38\times10^{-5}\frac{1}{(E_{vp}[\text{eV}])^4}\frac{(\tau_A[\text{s}])^{-1}\sigma_B^{++}[\text{Mb}]}{(R[\text{Å}])^6}, \tag{41}$$

as well as the relationship between lifetime and width,

$$\tau[\text{s}] = 6.58\times10^{-16}\frac{1}{\Gamma[\text{eV}]}. \tag{42}$$

The radiative lifetime of $Mg^+(2p^{-1})$ is 0.2 ns, while due to ICD alone the lifetime of this ion inside C_{60} becomes 770 fs. Even dICD alone would reduce the lifetime of $Mg^+(2p^{-1})$@C_{60} to the ps time regime (3.1 ps). Clearly, dICD is a relevant process in Mg@C_{60} after $2p$ ionization. For completeness, we mention that the ion $Mg^+(2p^{-1})$, unlike $Ne^+(2s^{-1})$, can also decay by autoionization [58,59].

Having seen that dICD can be an efficient decay pathway in Mg@C_{60}, we now turn to He@C_{60} where after the lowest excitation $1s \rightarrow 2p$ of He, ICD as well as dICD are open decay channels. Since there is no Coulomb repulsion in the final state, the excess energy of 21.2 eV is sufficient to trigger the double ionization of C_{60} by energy transfer. Here, except for radiative decay, there is no competition to ICD and dICD by other decay mechanisms. ICD is very efficient for this system; its lifetime is only 3.5 fs as compared to the radiative lifetime of 0.56 ns in the isolated excited He atom. Keeping in mind that the asymptotic expression overestimates ICD lifetimes, the correct value might be sub-fs. dICD is also efficient and would by itself lead the short lifetime of 0.29 ps, more than two orders of magnitude shorter than the radiative lifetime.

Having seen that dICD, depending on the system and neighbor chosen, can be an efficient process, orders of magnitude faster than radiative decay, we concentrate in the following on the ratio of the dICD and ICD rates. From the asymptotic expressions for these rates, it is obvious that their ratio is simply provided by the ratio of the double- to single-ionization cross sections at the respective excess energy:

$$\frac{\Gamma_{\rm dICD}}{\Gamma_{\rm ICD}} = \frac{\sigma_B^{++}}{\sigma_B^{+}}. \tag{43}$$

Consequently, the dICD to ICD ratio is determined by the cross sections of the neighbor alone, while the state of the decaying system determines the photon energy at which these

TABLE II. Ratio of the photoionization to single-photon double-ionization cross sections for selected atoms and molecules. In the first column are the atomic or molecular species listed, in the second are their double-ionization potentials (DIP), in the third are the single-photon double-ionization (SPDI) to photoionization (PI) ratios at specific photon energies, and the last contains the corresponding references. The photon energies are chosen as follows: 68.3 eV corresponds to the $4d^{-1}$ vacancy of Xe and 47.5 eV, 36.5 eV, 28.5 eV, and 275 eV give the highest cross section ratios of Be, Mg, Ca, and selenophene, respectively, in the available range. Data at other photon energies can be found in the respective references. The single-photon double-ionization to photoionization ratios are ratios of the respective cross sections or, if not available, ratios of the respective doubly to singly charged ions; the second case is marked with an asterisk (*).

Species	DIP (eV)	$\frac{\sigma_B^{++}(\omega)}{\sigma_B^{+}(\omega)}$ (%)	References
Na	52.4	0.9 (68.3 eV)	[60–62]
K	36.0	40 (68.3 eV)	[61]
Be	27.5	2.4 (47.5 eV)	[14,15]
Mg	22.7	0.9 (36.5 eV)	[5,14–16]
Ca	18.0	4.0 (28.5 eV)	[14]
C_6H_6	26.1	23 (68.3 eV)*	[19]
$C_6H_6D_3$	26.0	5 (68.3 eV)*	[13,19]
selenophene	24.2	80 (275 eV)*	
		10 (68.3 eV)*	[13,19]
pyrrole	24.2	11.2 (68.3 eV)*	[13,19]
furan	25.2	7.8 (68.3 eV)*	[13,19]
naphthalene	21.4	9 (68.3 eV)*	[13,19]
anthracene	20.1	13 (68.3 eV)*	[13,19]
pentancene	18.6	31 (68.3 eV)*	[13,19]
coronene	18.8	27.5 (68.3 eV)*	[13,19,54]
pyrene	19.3	19 (68.3 eV)*	[13,19,54]
C_{60}	19.0	49 (68.3 eV)	[53,55]

cross sections have to be taken. Having this in mind, we discuss in the following further simple examples of systems with high dICD to ICD ratios.

Table II gives an overview of doubly ionized species, their double-ionization potential (DIP), and their single-photon double-ionization (SPDI) to photoionization (PI) ratio at a specific photon energy, and it lists the corresponding publications from which the data were taken. The SPDI to PI ratio can be either the ratio of cross sections $\sigma_B^{++}/\sigma_B^{+}$ or the number of doubly to singly ionized ions M^{2+}/M^{+}. For C_{60} the respective cross sections are available, but not for the hydrocarbons listed. In the absence of autoionization, the amount of singly and doubly charged ions is proportional to their respective cross sections, and thus, the ratio of doubly to singly charged ions is equivalent to the ratio of the SPDI to PI cross sections and we will not distinguish between them in the following [11,19,63–66]. The photon energy of 68.3 eV used in most of the entries of the table is the excess energy of $Xe^{+}(4d^{-1})$ and just chosen as an example. Many more values are available in the literature cited. Before proceeding with the discussion, a short comment on the ratios of Mg and Ca in the table is in order. Both ratios are the highest ones in the measured or calculated photon energy range. The SPDI cross section of Mg is measured and calculated from threshold to about 54 eV [5,14–16,54,67] and the ratio reaches its highest point of 0.9% at 36.5 eV. The ratio for Ca is calculated up to 43 eV and has its highest value of 4% at 28.5 eV [14,67].

As seen in Table II, aromatic hydrocarbons—benzene, naphthalene, anthracene, pentacene, pyrene, coronene, pyrrole, furan, and selenophene—are suitable neighbors and offer rather low-lying double-ionization thresholds, ranging from 18.6 eV to 26.1 eV. These molecules play an important role in astrophysics [68–70]. Experimental investigations as in Refs. [13,19] show that the ratios of doubly charged to singly charged ions can reach values up to nearly 80% (selenophene) for photon energies above 200 eV. For a photon energy of 68.3 eV, which is the excess energy of the $4d^{-1}$ vacancy of Xe, the ratio is much smaller, but still reaches 23% for benzene, 31% for pentacene, and even 49% for C_{60}.

For even smaller excess energies, the SPDI to PI ratio typically further decreases. Nevertheless, dICD can still be efficient. In the following, we discuss briefly two sets of examples. In the first, the decaying system is Ne^{+} in the state $2s^2 2p^4(^1D)3s$ which has an excess energy of 30.5 eV [52] and its radiative rate is $w_A = 1.4 \times 10^9$ 1/s [71]. This state is populated by Auger decay [72–74].

We focus on the systems Ne^{+}-coronene, Ne^{+}-pyrene, and Ne^{+}-pentacene. Intermolecular distances between Ne^{+} and aromatic hydrocarbons typically range from 3 Å to 3.5 Å [75–77]. Coronene has a double-ionization threshold of 18.8 eV, while pyrene has one of 19.3 eV. Their ratios of SPDI to PI or the dICD to ICD ratio at 30.5 eV are about 5.9% and 9%, respectively [13,19,54]. The double-ionization threshold of pentacene lies at 18.6 eV and the SPDI to PI ratio at 30.5 eV reaches 10% [13,19,54]. Even for photon energies near the threshold, the dICD to ICD ratios are sizable for aromatic hydrocarbons. We would like to stress that Ne^{+} in the state $2s^2 2p^4(^1D)3s$ cannot undergo autoionization and hence there are no competitive processes present.

In the second set of examples, we combine the excited $(1s \rightarrow 2p)$ helium ion He^{+} [78] with coronene, pyrene, and pentacene. This ion has been utilized to investigate ICD in the extreme He dimer [79,80]. The $2p \rightarrow 1s$ transition provides an excess energy of 40.8 eV. The dICD to ICD ratios for this virtual photon energy become 13.7% for coronene, 12.1% for pyrene, and even 19% for pentacene [13,19,54]. These high ratios make clear that dICD can be a significant percentage of ICD for photon energies not close to the double-ionization threshold.

Since SPDI can be large at larger photon energies (see, e.g., selenophene in Table II), the dICD to ICD ratio can become very large for these energies. However, as the excess energy enters the asymptotic expression to the fourth power in the denominator, the absolute impact of dICD is still expected to be small at high values of the energy. Large virtual photon energies are present in core ionization and excitation processes which preferentially decay by Auger. In clusters and the condensed phase, however, core ICD competes with Auger decay. In rare gas clusters, the ICD to Auger decay ratio has recently been found to nevertheless amount to around 1% in Ar and to a few percent in Xe clusters [78,81]. The timescale of the core level ICD was determined to be 33 fs for the 2p core hole of aqueous Ca^{2+} implying that the ICD to Auger

decay ratio can be around 10% [82]. All of this gives hope that dICD may be a relevant process in core ionization and excitation in extended systems.

After having demonstrated that dICD can be a significant decay channel depending on the system and its neighbor, we discuss the influence of several neighbors. For ICD it has been shown that the decay width of the system increases with increasing number N of the surrounding neighbors [34,83–85]. A linear behavior with N was found in $NeHe_N$ and $CaHe_N$ clusters [84], while in $Na^+(H_2O)_N$ and $Mg^{2+}(H_2O)_N$ it was shown that the decay width deviates from a linear behavior [85], due to the polarization of water by the charged ions. Each water molecule becomes polarized by the alkali ion and shields the ion's charge from the other water molecules. Every additional water molecule becomes less polarized due to the shielding of the charge and gives a smaller contribution to the total ICD width. Consequently, further water molecules get less and less polarized and their contributions decrease with increasing N. The effect increases for higher-charged ions. However, for a small number of neighbors, a linear increase of the ICD width scaling with N can be assumed [84,85]. From the asymptotic equation, one obtains a linear growth with the number N of equivalent neighbors of the rate of dICD as well as long as the neighbors do not interact with each other. Once the neighbors do interact with each other and/or the intermolecular distances are too short for the asymptotic expression to be valid, the dICD rate grows with N, but the behavior as a function of N will depend on the situation at hand and has still to be investigated.

For completeness, we finally briefly mention other interatomic or intermolecular processes where two electrons can be emitted. As explained above for $Ne@C_{60}$, the excess energy of Ne after $2s$ ionization is insufficient for dICD to take place. However, another process can take place which has been termed dETMD [20] (ETMD stands for electron transfer mediated decay [48]). The process $Ne^+(2s^{-1})@C_{60} \rightarrow Ne@C_{60}^{3+} + 2e^-$ gives rise to a neutral Ne and a triply charged C_{60} cage, whereby two electrons have been emitted in concert [20]. Doubly excited states, for instance of He [86,87], possess sufficient excess energy to undergo dICD with various neighbors. Since two electrons are excited, the process is expected to be sequential rather than nonsequential in this case. Another interesting two-step process can also take place with doubly excited species. The doubly excited species can first autoionize and the resulting ion can then undergo ETMD with a neighbor [88]. As a consequence, two electrons have been emitted, one from the species carrying the excess energy and one from the neighbor.

IV. CONCLUSIONS

The double-ionization mechanism by interatomic or intermolecular Coulombic decay, briefly called dICD, is investigated. For large separations between the atom or molecule carrying the excess energy and its neighbor, an explicit asymptotic expression for the decay rate of dICD has been derived which solely depends on experimentally measurable quantities. This decay width provides a lower bound to the full dICD width and is a useful estimate of the exact total dICD width. The asymptotic expression is applied to several examples showing that dICD is a relevant decay channel. Within the asymptotic expressions, the dICD to ICD ratio corresponds to the ratio of the cross sections of single-photon double and single ionization. The knowledge of this ratio for various photon energies can thus help to choose atoms and molecules for which the ratio of dICD to ICD is favorable. The probability that an atom absorbs a resonant photon and emits a virtual photon is much higher than that to directly double-ionize an atom or molecule by the same photon. Consequently, doubly ionizing a system in an environment via dICD can become a more relevant process than SPDI. As for ICD, it is argued that the dICD rate grows substantially with the number of neighbors which can be doubly ionized by the available excess energy. This fact can make dICD important in true environments where the number of available neighbors is usually high.

Apart from the analysis of the asymptotic expression, we developed an analytical expression for the scattering T matrix of dICD which is valid for smaller distances between the species by using many-body perturbation theory. This results in a comprehensive expression for the total decay width of dICD, allowing one to distinguish various different intra- and interatomic and molecular processes. To further analyze the resulting perturbative decay width, we considered it in the limit of separated subsystems, which reduces the expression to the asymptotic formula. While the asymptotic dICD width accounts only for processes like knock-out, shake-off, and ground-state correlations, which are familiar from the discussion of the single-photon double ionization, the perturbative dICD width contains further mechanisms which are important at shorter interatomic distances. A different *ab initio* method (Fano-ADC), which belongs to a family of *ab initio* techniques for computing electronic decay widths, has been successfully applied to various ICD processes [89–92]. Recently, an ADC(2,2) approximation was introduced which has the potential to describe dICD of energetic singly ionized states [32]. Further development and implementation of these numerical techniques is necessary to investigate the qualitative and quantitative influence of these additional processes. It is beyond the scope of the present work and is left for the future.

We briefly mention what one could calculate in addition to the rates once the many-body perturbation theory is implemented. The ejected electron spectra can be computed by using the differential partial decay width [Eq. (32)]. It should be clear that this can only be done after the many-body perturbation theory is implemented, which is a large effort by itself because of the two electrons in the continuum and that not for a spherical system. To compare with experiment one has also to take into account the impact of the nuclear motion in the dICD undergoing system as done before for ICD. This requires additional method development. However, in many cases a comparison can be done without the inclusion of the nuclear motion if we assume instantaneous decay and small energy broadening due to the distribution of the interatomic distances in the vibrational wave packet compared to the total energy of the two emitted electrons. Both assumptions hold for the systems we considered. The total decay width is of order of several meV and is larger than

the characteristic frequencies in the decaying state, while the total energy of the emitted electrons is larger than several eV. Under these assumptions we may resort to Eq. (32) as such. Beyond the dICD electron spectra, triply differential cross sections can be computed as well from the absolute value squared of the dICD amplitude [see Eq. (31)] analogously to the case of the one-photon double-ionization process as shown in [93–95].

We hope our work will prepare the ground for further discussion and research into dICD.

ACKNOWLEDGMENTS

We want to thank J. Schirmer for helpful discussions and a critical reading of the manuscript. Furthermore, we would like to thank I. Bray, A. S. Kheifets, and R. Wehlitz for providing theoretical and experimental data. Financial support by the European Research Council (ERC) (Advanced Investigator Grant No. 692657) and the US ARO (Grant No. W911NF-14-1-0383) is gratefully acknowledged.

APPENDIX A: TRANSITION AMPLITUDE OF dICD VIA MANY-BODY PERTURBATION THEORY

In this Appendix, we present the complete second-order transition amplitude of our system $T^{(2)}_{\varepsilon_k\varepsilon_{k'}ov_Aov_Bov'_B}$ which comprises eighteen terms and we explain how it is structured. As discussed in Sec. II B, we impose the condition that our decaying state $|\Phi_{iv_A}\rangle$ and our final state $|\Phi^{\varepsilon_k\varepsilon_{k'}}_{ov_Aov_Bov'_B}\rangle$ are orthogonal. The orthogonality condition is automatically fulfilled for zeroth and first order. Since our transition amplitude is second order, the initial and final states have to be also orthogonal through second order, which is equivalent to setting the following scalar products to zero:

$$\left\langle \Psi^{(0)}_{\varepsilon_k\varepsilon_{k'}ov_Aov_Bov'_B}\middle|\Psi^{(2)}_{iv_A}\right\rangle = \left\langle \Phi^{\varepsilon_k\varepsilon_{k'}}_{ov_Aov_Bov'_B}\middle|\frac{\hat{Q}_D}{E^{(0)}_{iv_A}-\hat{H}_0}\hat{H}_I\frac{\hat{Q}_D}{E^{(0)}_{iv_A}-\hat{H}_0}\hat{H}_I\middle|\Phi_{iv_A}\right\rangle, \tag{A1a}$$

$$\left\langle \Psi^{(2)}_{\varepsilon_k\varepsilon_{k'}ov_Aov_Bov'_B}\middle|\Psi^{(0)}_{iv_A}\right\rangle = \left\langle \Phi^{\varepsilon_k\varepsilon_{k'}}_{ov_Aov_Bov'_B}\middle|\hat{H}_I\frac{\hat{Q}_F}{E^{(0)}_{\varepsilon_k\varepsilon_{k'}ov_Aov_Bov'_B}-\hat{H}_0}\hat{H}_I\frac{\hat{Q}_F}{E^{(0)}_{\varepsilon_k\varepsilon_{k'}ov_Aov_Bov'_B}-\hat{H}_0}\middle|\Phi_{iv_A}\right\rangle, \tag{A1b}$$

$$\left\langle \Psi^{(1)}_{\varepsilon_k\varepsilon_{k'}ov_Aov_Bov'_B}\middle|\Psi^{(1)}_{iv_A}\right\rangle = \left\langle \Phi^{\varepsilon_k\varepsilon_{k'}}_{ov_Aov_Bov'_B}\middle|\hat{H}_I\frac{\hat{Q}_F}{E^{(0)}_{\varepsilon_k\varepsilon_{k'}ov_Aov_Bov'_B}-\hat{H}_0}\frac{\hat{Q}_D}{E^{(0)}_{iv_A}-\hat{H}_0}\hat{H}_I\middle|\Phi_{iv_A}\right\rangle. \tag{A1c}$$

This is achieved by constructing specific projectors $\hat{Q}_D$ and $\hat{Q}_F$, which we write as $\hat{Q} = \mathbb{1} - \sum_N |\Phi_N\rangle\langle\Phi_N|$, where the sum over N runs over some selected subspace of configurations. Many-body perturbation theory dictates that $\hat{Q}_D$ and $\hat{Q}_F$ do not contain $|\Phi_{iv_A}\rangle$ and $|\Phi^{\varepsilon_k\varepsilon_{k'}}_{ov_Aov_Bov'_B}\rangle$, respectively, which otherwise would result in vanishing energy denominators. To ensure that the first two expressions in Eqs. (A1a) and (A1b) are zero we introduce further restrictions on the projection operators and exclude $|\Phi^{\varepsilon_k\varepsilon_{k'}}_{ov_Aov_Bov'_B}\rangle\langle\Phi^{\varepsilon_k\varepsilon_{k'}}_{ov_Aov_Bov'_B}|$ and $|\Phi_{iv_A}\rangle\langle\Phi_{iv_A}|$ from $\hat{Q}_D$ and $\hat{Q}_F$, respectively. To make the third expression [Eq. (A1c)] vanish we first determine all virtual states $|\Phi_K\rangle$ such that the amplitude $\langle\Psi^{(1)}_{\varepsilon_k\varepsilon_{k'}ov_Aov_Bov'_B}|\Psi^{(1)}_{iv_A}\rangle = \langle\Phi^{\varepsilon_k\varepsilon_{k'}}_{ov_Aov_Bov'_B}|\frac{\hat{H}_I}{E^{(0)}_{\varepsilon_k\varepsilon_{k'}ov_Aov_Bov'_B}-\hat{H}_0}|\Phi_K\rangle\langle\Phi_K|\frac{\hat{H}_I}{E^{(0)}_{iv_A}-\hat{H}_0}|\Phi_{iv_A}\rangle$ is nonzero. The contributing virtual states are 1p2h and 2p3h states, listed in Tables III and IV. 1h states would vanish, because the contribution of the averaged potential $\hat{v}^{HF}$ and the one-particle contribution of the Coulomb operator $\hat{V}$ cancel each other in the Hartree-Fock approximation: $\langle\Phi_n|\hat{H}_I|\Phi_{iv_A}\rangle = v^{HF}_{n\,iv_A} + \sum_k V_{nk[iv_A\,k]} = 0$ [96,97]. Note that one of the holes of the 2p3h states has to be iv_A, so that only four spin orbitals change during one transition and the coupling to the initial 1h state $|\Phi_{iv_A}\rangle$ via the two-particle Coulomb operator is possible.

To ensure orthogonality in second order, the above configurations of the inserted virtual states cannot be simultaneously present in $\hat{Q}_D$ and $\hat{Q}_F$. Therefore, we divide the set $|\Phi_N\rangle$ into two disjoint subsets which are included either in $\hat{Q}_D$ or in $\hat{Q}_F$. The choice of the subsets is not unique, but it does not affect the expression for the transition amplitude. In the following, we want to show two different possibilities for dividing into subsets.

In the first division, we use the definition of a bound state in continuum. The decaying state $|\Psi_{iv_A}\rangle$ is such a state, which means it should decay exponentially for $\boldsymbol{r}_i \to \infty$ ($\boldsymbol{r}_i$ is the spatial coordinate of electron i). By allowing continuum states into the decaying state expansion this boundary condition cannot be fulfilled any longer. Therefore, we select $\hat{Q}_D$ such that no continuum states can appear in the decaying state expansion. Consequently, $\hat{Q}_D$ does not include virtual states as in Tables III and IV, while $\hat{Q}_F$ comprises them all.

In the second division, we follow the many-body perturbation theory treatment of the double Auger and SPDI processes [2,3,6]. Therefore, we remove all 1p2h states (see

TABLE III. Virtual 1p2h states which couple the initial and final state in second order. Free index h (p) runs over all occupied (unoccupied) orbitals.

	$\sum_p$	$\sum_h$
1	$\Phi^{p}_{ov_Aov_B}$	$\Phi^{\varepsilon_k}_{ov_Ah}$
2	$\Phi^{p}_{ov_Bov'_B}$	$\Phi^{\varepsilon_k}_{ov_Bh}$
3	$\Phi^{p}_{ov'_Bov_A}$	$\Phi^{\varepsilon_k}_{ov'_Bh}$
4		$\Phi^{\varepsilon_{k'}}_{ov_Ah}$
5		$\Phi^{\varepsilon_{k'}}_{ov_Bh}$
6		$\Phi^{\varepsilon_{k'}}_{ov'_Bh}$

TABLE IV. Virtual 2p3h states which couple the initial and final state in second order. Free index h (p) runs over all occupied (unoccupied) orbitals.

	$\sum_p$	$\sum_h$
1	$\Phi^{\varepsilon_k p}_{ov_A ov_B iv_A}$	$\Phi^{\varepsilon_k \varepsilon_{k'}}_{ov_A hiv_A}$
2	$\Phi^{\varepsilon_k p}_{ov_B ov'_B iv_A}$	$\Phi^{\varepsilon_k \varepsilon_{k'}}_{ov_B hiv_A}$
3	$\Phi^{\varepsilon_k p}_{ov'_B ov_A iv_A}$	$\Phi^{\varepsilon_k \varepsilon_{k'}}_{ov'_B hiv_A}$
4	$\Phi^{p \varepsilon_{k'}}_{ov_A ov_B iv_A}$	
5	$\Phi^{p \varepsilon_{k'}}_{ov_B ov'_B iv_A}$	
6	$\Phi^{p \varepsilon_{k'}}_{ov'_B ov_A iv_A}$	

Table III) from $\hat{Q}_D$ and all 2p3h states (see Table IV) from $\hat{Q}_F$. This procedure is in conformity with the derivation of transition amplitudes for double Auger and SPDI. In double Auger including the corresponding 1p2h and 2p3h states results in negligible contributions to transition amplitudes due to large energy denominators and small Coulomb integrals. In the description of the SPDI process, the initial state contains no 1p2h configurations due to Brillouin's theorem [96], while in the final-state expansion the 2p3h configurations do not contribute because they do not couple to the ground state via the dipole operator (see Appendix C). If we consider the asymptotic dICD amplitude [see Eq. (21) in Sec. II A] this procedure for constructing the SPDI states directly translates into the second division of the set $|\Phi_N\rangle$. We would also like to mention that without enforcing orthogonality through second order, an additional factor 2 appears in the transition amplitude, because the perturbative expansions of the initial and the final states produce the same contribution.

Returning to the derivation of the transition amplitude, we insert the resolution of unperturbed states into Eq. (26) and evaluate the Coulomb integrals. The transition amplitude is finally given by

$$
\begin{aligned}
T^{(2)}_{\varepsilon_k \varepsilon_{k'} ov_A ov_B ov'_B; iv_A} = \sum_p \Bigg[& \frac{V_{\varepsilon_k \varepsilon_{k'}\,[ov'_B\, p]}}{\varepsilon_k + \varepsilon_{k'} - \varepsilon_{ov'_B} - \varepsilon_p + i0^+} V_{p\, iv_A\,[ov_A\, ov_B]} + \frac{V_{\varepsilon_k \varepsilon_{k'}\,[ov_A\, p]}}{\varepsilon_k + \varepsilon_{k'} - \varepsilon_{ov_A} - \varepsilon_p + i0^+} V_{p\, iv_A\,[ov_B\, ov'_B]} \\
& + \frac{V_{\varepsilon_k \varepsilon_{k'}\,[ov_B\, p]}}{\varepsilon_k + \varepsilon_{k'} - \varepsilon_{ov_B} - \varepsilon_p + i0^+} V_{p\, iv_A\,[ov'_B\, ov_A]} \Bigg] + \sum_h \Bigg[-V_{iv_A\, \varepsilon_k\,[ov_A\, h]} \frac{V_{h\, \varepsilon_{k'}\,[ov_B\, ov'_B]}}{\varepsilon_h + \varepsilon_{k'} - \varepsilon_{ov_B} - \varepsilon_{ov'_B}} \\
& - V_{iv_A\, \varepsilon_k\,[ov_B\, h]} \frac{V_{h\, \varepsilon_{k'}\,[ov'_B\, ov_A]}}{\varepsilon_h + \varepsilon_{k'} - \varepsilon_{ov'_B} - \varepsilon_{ov_A}} - V_{iv_A\, \varepsilon_k\,[ov'_B\, h]} \frac{V_{h\, \varepsilon_{k'}\,[ov_A\, ov_B]}}{\varepsilon_h + \varepsilon_{k'} - \varepsilon_{ov_A} - \varepsilon_{ov_B}} + V_{iv_A\, \varepsilon_{k'}\,[ov_A\, h]} \frac{V_{h_B\, \varepsilon_k\,[ov_B\, ov'_B]}}{\varepsilon_h + \varepsilon_k - \varepsilon_{ov_B} - \varepsilon_{ov'_B}} \\
& + V_{iv_A\, \varepsilon_{k'}\,[ov_B\, h]} \frac{V_{h_B\, \varepsilon_k\,[ov'_B\, ov_A]}}{\varepsilon_h + \varepsilon_k - \varepsilon_{ov'_B} - \varepsilon_{ov_A}} + V_{iv_A\, \varepsilon_{k'}\,[ov'_B\, h]} \frac{V_{h\, \varepsilon_k\,[ov_A\, ov_B]}}{\varepsilon_h + \varepsilon_k - \varepsilon_{ov_A} - \varepsilon_{ov_B}} \Bigg] \\
& + \sum_p \Bigg[V_{iv_A\, \varepsilon_{k'}\,[ov'_B\, p]} \frac{V_{p\, \varepsilon_k\,[ov_A\, ov_B]}}{\varepsilon_p + \varepsilon_k - \varepsilon_{ov_A} - \varepsilon_{ov_B}} + V_{iv_A\, \varepsilon_{k'}\,[ov_A\, p]} \frac{V_{p\, \varepsilon_k\,[ov_B\, ov'_B]}}{\varepsilon_p + \varepsilon_k - \varepsilon_{ov_B} - \varepsilon_{ov'_B}} \\
& + V_{iv_A\, \varepsilon_{k'}\,[ov_B\, p]} \frac{V_{p\, \varepsilon_k\,[ov'_B\, ov_A]}}{\varepsilon_p + \varepsilon_k - \varepsilon_{ov'_B} - \varepsilon_{ov_A}} - V_{iv_A\, \varepsilon_k\,[ov'_B\, p]} \frac{V_{p\, \varepsilon_{k'}\,[ov_A\, ov_B]}}{\varepsilon_p + \varepsilon_{k'} - \varepsilon_{ov_A} - \varepsilon_{ov_B}} - V_{iv_A\, \varepsilon_k\,[ov_A\, p]} \frac{V_{p\, \varepsilon_{k'}\,[ov_B\, ov'_B]}}{\varepsilon_p + \varepsilon_{k'} - \varepsilon_{ov_B} - \varepsilon_{ov'_B}} \\
& - V_{iv_A\, \varepsilon_k\,[ov_B\, p]} \frac{V_{p\, \varepsilon_{k'}\,[ov'_B\, ov_A]}}{\varepsilon_p + \varepsilon_{k'} - \varepsilon_{ov'_B} - \varepsilon_{ov_A}} \Bigg] + \sum_h \Bigg[\frac{V_{\varepsilon_k \varepsilon_{k'}\,[ov_A\, h]}}{\varepsilon_k + \varepsilon_{k'} - \varepsilon_{ov_A} - \varepsilon_h} V_{h\, iv_A\,[ov_B\, ov'_B]} \\
& + \frac{V_{\varepsilon_k \varepsilon_{k'}\,[ov_B\, h]}}{\varepsilon_k + \varepsilon_{k'} - \varepsilon_{ov_B} - \varepsilon_h} V_{h\, iv_A\,[ov'_B\, ov_A]} + \frac{V_{\varepsilon_k \varepsilon_{k'}\,[ov'_B\, h]}}{\varepsilon_k + \varepsilon_{k'} - \varepsilon_{ov'_B} - \varepsilon_h} V_{h\, iv_A\,[ov_A\, ov_B]} \Bigg]. \qquad \text{(A2)}
\end{aligned}
$$

The total expression for the perturbative dICD transition amplitude in Eq. (A2) is structured as follows. The first two sums feature the coupling of the initial hole state to the 1p2h states (as in Fig. 3), whereby the first sum over particle orbitals in the continuum has a singularity as explained in Sec. II B. The first sum over particle orbitals and the second over hole orbitals are the knock-out and the shake-off amplitudes, respectively. The 3rd and 4th sums correspond to the coupling to the unperturbed 2p3h states with one hole in iv_A (as in Fig. 4) and belong to the ground-state-correlation mechanisms.

APPENDIX B: THE LIMIT $R \to \infty$ OF THE PERTURBATIVELY DERIVED EXPRESSION FOR Γ_{dICD}

In the following, we want to show the perturbatively derived transition amplitude in the various processes of A and B for $R \to \infty$ in more detail than in Sec. II B. Assuming a large distance R between the species makes several assumptions valid. All terms with a Coulomb integral corresponding to electron transfer, as for example $+\sum_p V_{\varepsilon_k \varepsilon_{k'}\,[ov_A\, p]} \left(\frac{1}{\varepsilon_k + \varepsilon_{k'} - \varepsilon_{ov_A} - \varepsilon_p + i0^+}\right) V_{p\, iv_A\,[ov_B\, ov'_B]}$, can be neglected because they decay exponentially with R. The second

Coulomb integral describes electron transfer independent of the localization site of p. Note that other Coulomb integrals also describe electron transfer, if the appearing sum runs only over hole or particle states of A, like in $-\sum_{h_A} V_{iv_A\,\varepsilon_k\,[ov_A\,h_A]} V_{h_A\,\varepsilon_{k'}\,[ov_B\,ov'_B]} \left(\frac{1}{\varepsilon_{h_A}+\varepsilon_{k'}-\varepsilon_{ov_B}-\varepsilon_{ov'_B}}\right)$ [compare Eq. (28)], while the sum of states on B by itself gives a nonvanishing contribution. If electron transfer is neglected the Coulomb exchange terms presenting nonlocal processes vanish, too. In this case, the corresponding antisymmetrization brackets in the 4-index integrals can be skipped. We expand the interaction Coulomb operator $\hat{V}_{AB}$ [see Eq. (35)] and take the leading term which behaves as R^{-3}. Concerning B, only matrix elements presenting local processes are left, which are independent of R. Therefore, all leading terms are combinations of an interaction between A and B and a local process on B and scale as R^{-3}. In these approximations, the transition amplitude, Eq. (B1), takes on the form

$$
\begin{aligned}
T^{(R\to\infty)}_{\varepsilon_k\varepsilon_{k'}ov_Aov_Bov'_B;iv_A} = \sum_{p_B}\Bigg[& -\frac{V_{\varepsilon_k\,\varepsilon_{k'}\,[ov'_B\,p_B]}}{\varepsilon_k+\varepsilon_{k'}-\varepsilon_{ov'_B}-\varepsilon_{p_B}+i0^+} V_{p_B\,iv_A\,ov_B\,ov_A} + \frac{V_{\varepsilon_k\,\varepsilon_{k'}\,[ov_B\,p_B]}}{\varepsilon_k+\varepsilon_{k'}-\varepsilon_{ov_B}-\varepsilon_{p_B}+i0^+} V_{p_B\,iv_A\,ov'_B\,ov_A}\Bigg] \\
& + \sum_{h_B}\Bigg[-V_{iv_A\,\varepsilon_k\,ov_A\,h_B}\frac{V_{h_B\,\varepsilon_{k'}\,[ov_B\,ov'_B]}}{\varepsilon_{h_B}+\varepsilon_{k'}-\varepsilon_{ov_B}-\varepsilon_{ov'_B}} + V_{iv_A\,\varepsilon_{k'}\,ov_A\,h_B}\frac{V_{h_B\,\varepsilon_k\,[ov_B\,ov'_B]}}{\varepsilon_{h_B}+\varepsilon_k-\varepsilon_{ov_B}-\varepsilon_{ov'_B}}\Bigg] \\
& + \sum_{p_B}\Bigg[V_{iv_A\,\varepsilon_{k'}\,ov_A\,p_B}\frac{V_{p_B\,\varepsilon_k\,[ov_B\,ov'_B]}}{\varepsilon_{p_B}+\varepsilon_k-\varepsilon_{ov_B}-\varepsilon_{ov'_B}} - V_{iv_A\,\varepsilon_k\,ov_A\,p_B}\frac{V_{p_B\,\varepsilon_{k'}\,[ov_B\,ov'_B]}}{\varepsilon_{p_B}+\varepsilon_{k'}-\varepsilon_{ov_B}-\varepsilon_{ov'_B}}\Bigg] \\
& + \sum_{h_B}\Bigg[\frac{V_{\varepsilon_k\,\varepsilon_{k'}\,[ov_B\,h_B]}}{\varepsilon_k+\varepsilon_{k'}-\varepsilon_{ov_B}-\varepsilon_{h_B}} V_{h_B\,iv_A\,ov'_B\,ov_A} - \frac{V_{\varepsilon_k\,\varepsilon_{k'}\,[ov'_B\,h_B]}}{\varepsilon_k+\varepsilon_{k'}-\varepsilon_{ov'_B}-\varepsilon_{h_B}} V_{h_B\,iv_A\,ov_B\,ov_A}\Bigg].
\end{aligned}
\tag{B1}
$$

The Coulomb integrals describing the interaction between A and B read

$$
V_{p_Biv_Ah_Bov_A} = \iint \varphi^*_{iv_A}(\boldsymbol{r}^{(A)})\varphi^*_{p_B}(\boldsymbol{r}^{(B)})\,\frac{e^2}{|\boldsymbol{r}^{(B)}-\boldsymbol{r}^{(A)}|}\,\varphi_{ov_A}(\boldsymbol{r}^{(A)})\varphi_{h_B}(\boldsymbol{r}^{(B)})\,d\boldsymbol{r}^{(A)}d\boldsymbol{r}^{(B)}. \tag{B2}
$$

As described above, the interaction Coulomb operator can be multipole-expanded for $R\to\infty$ [see Eq. (7)], where the expansion is broken off after the dipole term, which is the first giving a contribution. Choosing $\boldsymbol{e_R}=\boldsymbol{e_z}$ and inserting the expansion $\hat{v}_{AB}\approx e^2/R^3[\boldsymbol{\xi r}-3(\boldsymbol{\xi e_R})(\boldsymbol{r e_R})]$ into Eq. (B2) gives

$$
V_{p_Biv_Ah_Bov_A} \approx \frac{1}{R^3}\left[\langle\varphi_{iv_A}|\hat{d}_x{}^{(A)}|\varphi_{ov_A}\rangle\langle\varphi_{p_B}|\hat{d}_x{}^{(B)}|\varphi_{h_B}\rangle + \langle\varphi_{iv_A}|\hat{d}_y{}^{(A)}|\varphi_{ov_A}\rangle\langle\varphi_{p_B}|\hat{d}_y{}^{(B)}|\varphi_{h_B}\rangle - 2\,\langle\varphi_{iv_A}|\hat{d}_z{}^{(A)}|\varphi_{ov_A}\rangle\langle\varphi_{p_B}|\hat{d}_z{}^{(B)}|\varphi_{h_B}\rangle\right], \tag{B3}
$$

where $\hat{d}_x$, $\hat{d}_y$, and $\hat{d}_z$ are the components of the one-particle dipole operator. The Coulomb integrals of the form $V_{p_Biv_Ah_Bov_A}$ in Eq. (B1) are replaced by the approximation of Eq. (B3). For simplicity, we only show the transformations of the perturbative amplitude by the first term of Eq. (B1), P_1. The procedure is analogous for the other terms and thus, we can later generalize our findings to get the total transition amplitude. After inserting the expansion of the interaction Coulomb operator, P_1 becomes

$$
P_1 = \frac{1}{R^3}T_1 = \frac{1}{R^3}\left[\langle\varphi_{iv_A}|\hat{d}_x{}^{(A)}|\varphi_{ov_A}\rangle T_x^{(B)} + \langle\varphi_{iv_A}|\hat{d}_y{}^{(A)}|\varphi_{ov_A}\rangle\,T_y^{(B)} - 2\,\langle\varphi_{iv_A}|\hat{d}_z{}^{(A)}|\varphi_{ov_A}\rangle\,T_z^{(B)}\right]. \tag{B4}
$$

$T_x^{(B)}$, $T_y^{(B)}$, and $T_z^{(B)}$ can be identified as the components of the single-photon double-ionization transition amplitude (see Refs. [2,3]) describing the knock-out mechanism:

$$
T_x^{(B)} = \sum_{p_B}\langle\varphi_{p_B}|\hat{d}_x{}^{(B)}|\varphi_{ov_B}\rangle\,\frac{V_{\varepsilon_k\,\varepsilon_{k'}\,[ov'_B\,p_B]}}{\varepsilon_k+\varepsilon_{k'}-\varepsilon_{p_B}-\varepsilon_{ov'_B}+i0^+}, \tag{B5a}
$$

$$
T_y^{(B)} = \sum_{p_B}\langle\varphi_{p_B}|\hat{d}_y{}^{(B)}|\varphi_{ov_B}\rangle\,\frac{V_{\varepsilon_k\,\varepsilon_{k'}\,[ov'_B\,p_B]}}{\varepsilon_k+\varepsilon_{k'}-\varepsilon_{p_B}-\varepsilon_{ov'_B}+i0^+}, \tag{B5b}
$$

$$
T_z^{(B)} = \sum_{p_B}\langle\varphi_{p_B}|\hat{d}_z{}^{(B)}|\varphi_{ov_B}\rangle\,\frac{V_{\varepsilon_k\,\varepsilon_{k'}\,[ov'_B\,p_B]}}{\varepsilon_k+\varepsilon_{k'}-\varepsilon_{p_B}-\varepsilon_{ov'_B}+i0^+}. \tag{B5c}
$$

For an atomic system, the absolute value squared of the transition amplitude T_1 in Eq. (B4) is averaged and summed over the spin and spatial degeneracies of the initial and the finals state, respectively,

$$
\overline{|T_1|^2} = \frac{1}{2\,l_{iv_A}+1}\frac{1}{2\,s_{iv_A}+1}\sum_{\substack{m_{l_{iv_A}}m_{l_{ov_A}}\\ m_{l_{ov_B}}m_{l_{ov'_B}}}}\sum_{\eta\lambda\delta\nu\mu\sigma}|T_1|^2, \tag{B6}
$$

where mixed terms vanish and quadratic terms give the same contribution, which leads to an additional factor 6 due to six quadratic terms of the transition amplitude. Therefore, we can rewrite Eq. (B6) in terms of the z component as

$$
\overline{|T_1|^2} = 6\,\overline{\left|\langle\varphi_{iv_A}|\hat{d}_z{}^{(A)}|\varphi_{ov_A}\rangle\,T_z^{(B)}\right|^2}. \tag{B7}
$$

Using the fact that the three components of the dipole operators give the same contribution allows us to rewrite $\overline{|\langle\varphi_{iv_A}|\hat{d}_z^{(A)}|\varphi_{ov_A}\rangle|^2} = (1/3)\overline{|\langle\varphi_{iv_A}|\hat{\boldsymbol{d}}_A|\varphi_{ov_A}\rangle|^2}$ and $\overline{|T_z^{(B)}|^2} = (1/3)\overline{|\boldsymbol{T}_B|^2}$ in terms of the full dipole operators. Finally, the first term P_1 [compare Eq. (B4)] of Eq. (B1) reads in its reduced form

$$P_1 = \frac{2}{3R^6}\overline{|\langle\varphi_{iv_A}|\hat{\boldsymbol{d}}_A|\varphi_{ov_A}\rangle\,\boldsymbol{T}_B|^2}. \tag{B8}$$

Returning to the complete transition amplitude and generalizing it gives

$$\overline{\left|T^{(R\to\infty)}_{\varepsilon_k\varepsilon_{k'}ov_Aov_Bov'_B;iv_A}\right|^2} = \frac{2}{3R^6}\overline{\left|\langle\varphi_{iv_A}|\hat{\boldsymbol{d}}_A|\varphi_{ov_A}\rangle[\boldsymbol{T}(KO)+\boldsymbol{T}(SO)+\boldsymbol{T}(GSC_p)+\boldsymbol{T}(GSC_h)]\right|^2}. \tag{B9}$$

As shown in Appendix C using many-body perturbation theory using the present nomenclature, $\boldsymbol{T}(KO)$, $\boldsymbol{T}(SO)$, $\boldsymbol{T}(GSC_p)$, and $\boldsymbol{T}(GSC_h)$ of Eq. (B9) are transition amplitudes (see Refs. [2,3]) of single-photon double ionization. The four transition amplitudes belong to the different mechanisms: knock-out (KO), shake-off (SO), and ground-state correlations (GSC_p/GSC_h). The transition amplitudes read

$$\boldsymbol{T}(KO) = \sum_{p_B}\left[\langle\varphi_{p_B}|\hat{\boldsymbol{d}}_B|\varphi_{ov_B}\rangle\frac{V_{\varepsilon_k\,\varepsilon_{k'}\,[ov'_B\,p_B]}}{\varepsilon_k+\varepsilon_{k'}-\varepsilon_{p_B}-\varepsilon_{ov'_B}+i0^+} - \langle\varphi_{p_B}|\hat{\boldsymbol{d}}_B|\varphi_{ov'_B}\rangle\frac{V_{\varepsilon_k\,\varepsilon_{k'}\,[ov_B\,p_B]}}{\varepsilon_k+\varepsilon_{k'}-\varepsilon_{p_B}-\varepsilon_{ov_B}+i0^+}\right], \tag{B10}$$

$$\boldsymbol{T}(SO) = \sum_{h_B}\left[\langle\varphi_{\varepsilon_k}|\hat{\boldsymbol{d}}_B|\varphi_{h_B}\rangle\frac{V_{h_B\,\varepsilon_{k'}\,[ov_B\,ov'_B]}}{\varepsilon_{k'}+\varepsilon_{h_B}-\varepsilon_{ov_B}-\varepsilon_{ov'_B}} - \langle\varphi_{\varepsilon_{k'}}|\hat{\boldsymbol{d}}_B|\varphi_{h_B}\rangle\frac{V_{h_B\,\varepsilon_k\,[ov_B\,ov'_B]}}{\varepsilon_k+\varepsilon_{h_B}-\varepsilon_{ov_B}-\varepsilon_{ov'_B}}\right], \tag{B11}$$

$$\boldsymbol{T}(GSC_p) = \sum_{p_B}\left[\langle\varphi_{\varepsilon_{k'}}|\hat{\boldsymbol{d}}_B|\varphi_{p_B}\rangle\frac{V_{p_B\,\varepsilon_k\,[ov_B\,ov'_B]}}{\varepsilon_k+\varepsilon_{p_B}-\varepsilon_{ov_B}-\varepsilon_{ov'_B}} - \langle\varphi_{\varepsilon_k}|\hat{\boldsymbol{d}}_B|\varphi_{p_B}\rangle\frac{V_{p_B\,\varepsilon_{k'}\,[ov_B\,ov'_B]}}{\varepsilon_{k'}+\varepsilon_{p_B}-\varepsilon_{ov_B}-\varepsilon_{ov'_B}}\right], \tag{B12}$$

$$\boldsymbol{T}(GSC_h) = \sum_{h_B}\left[\langle\varphi_{h_B}|\hat{\boldsymbol{d}}_B|\varphi_{ov'_B}\rangle\frac{V_{\varepsilon_k\,\varepsilon_{k'}\,[ov_B\,h_B]}}{\varepsilon_k+\varepsilon_{k'}-\varepsilon_{ov_B}-\varepsilon_{h_B}} - \langle\varphi_{h_B}|\hat{\boldsymbol{d}}_B|\varphi_{ov'_B}\rangle\frac{V_{\varepsilon_k\,\varepsilon_{k'}\,[ov'_B\,h_B]}}{\varepsilon_k+\varepsilon_{k'}-\varepsilon_{ov_B}-\varepsilon_{h_B}}\right]. \tag{B13}$$

The transition amplitude of SPDI consists of these four processes. The corresponding single-differential partial SPDI cross section is given by

$$\frac{d\sigma_B^{++}(\omega)}{d\varepsilon_{k'}} = \frac{4\pi^2}{3}\frac{\omega}{c}\sum_{ov_Bov'_B}\overline{|[T(KO)+T(SO)+T(GSC_p)+T(GSC_h)]|^2} \tag{B14}$$

and describes the single-photon double ionization of species B for photon energy $\hbar\omega$.

APPENDIX C: DERIVATION OF THE SPDI TRANSITION AMPLITUDE BY MANY-BODY PERTURBATION THEORY

The derivation of the dICD decay width is explained in the main text and the above appendices in much detail. Now, we want to derive the perturbative expression of the SPDI transition amplitude, which is already well known [2,3], in our nomenclature for the species B. As usual, the unperturbed initial and final state are Hartree-Fock ground states of B with annihilation and creation operators acting on them,

$$|\Phi_0\rangle = \left|\Phi_0^B\right\rangle, \tag{C1}$$

$$\left|\Phi^{\varepsilon_k\varepsilon_{k'}}_{ov_Bov'_B}\right\rangle = c^\dagger_{\varepsilon_k}c^\dagger_{\varepsilon_{k'}}c_{ov_B}c_{ov'_B}\left|\Phi_0^B\right\rangle, \tag{C2}$$

where B is initially in its ground state and finally doubly ionized, the two emitted electrons being indicated by ε_k and $\varepsilon_{k'}$ and the resulting holes by ov_B and ov'_B. Again, the Hartree-Fock approximation is applied in the context of perturbation theory. The initial and final states in zeroth order give no contribution. To obtain the transition amplitude $T^{(2)}_{\varepsilon_k\varepsilon_{k'}ov_Bov'_B}$ of SPDI, the states have to be expanded perturbatively through first order:

$$T^{(2)}_{\varepsilon_k\varepsilon_{k'}ov_Bov'_B} = \left\langle\Phi^{\varepsilon_k\varepsilon_{k'}}_{ov_Bov'_B}\middle|\hat{D}_B\frac{\hat{Q}_0}{E_0^{(0)}-\hat{H}_0^B}\hat{H}_I^B\middle|\Phi_0^B\right\rangle + \left\langle\Phi^{\varepsilon_k\varepsilon_{k'}}_{ov_Bov'_B}\middle|\hat{H}_I^B\frac{\hat{Q}_{\varepsilon_k\varepsilon_{k'}ov_Bov'_B}}{E^{(0)}_{\varepsilon_k\varepsilon_{k'}ov_Bov'_B}-\hat{H}_0^B}\hat{D}_B\middle|\Phi_0^B\right\rangle. \tag{C3}$$

Here, the first term is the initial-state expansion and the second term the final-state expansion. $\hat{Q}_0$ and $\hat{Q}_{\varepsilon_k\varepsilon_{k'}ov_Bov'_B}$ are projection operators of the form $\hat{Q} = \mathbb{1} - \sum_N |\Phi_N\rangle\langle\Phi_N|$ of the configurations iv_A and $\varepsilon_k\varepsilon_{k'}ov_Aov_Bov'_B$. $\hat{\boldsymbol{D}}_B$ and $\hat{H}_I$ are the dipole operator and the interaction Hamiltonian of B, respectively. The resolution of the unperturbed states in the form $\mathbb{1} = \sum_N |\Phi_N\rangle\langle\Phi_N|$, where N denotes the different configurations, is inserted to achieve the full expression of the SPDI transition amplitude. Formally, 1p1h and 2p2h states can be inserted. A closer look at the initial state expansion makes clear that only 2p2h states give a nonvanishing contribution. Matrix elements like $\langle\Phi^{p_1}_{h_1}|\hat{H}_I|\Phi_0\rangle$ vanish, because in Hartree-Fock, $\langle\Phi^{p_1}_{h_1}|\hat{H}_I|\Phi_0\rangle = v^{HF}_{p_1h_1} + \sum_k V_{p_1k[h_1\,k]} = 0$, as known from Brillouin's theorem [96]. In the final-state expansion only 1p1h states contribute, while for 2p2h-state terms the transition matrix elements vanish, $\langle\Phi^{\varepsilon_k\varepsilon_{k'}}_{ov_Bov'_B}|\hat{D}_B|\Phi_0\rangle = 0$,

as $\hat{\boldsymbol{D}}_B$ is a one-particle operator. After inserting the resolution of unperturbed states and evaluating the respective matrix elements, one gets the following expression for the SPDI transition amplitude:

$$
\begin{aligned}
T^{(2)}_{\varepsilon_k \varepsilon_{k'} o v_B o v'_B} = \sum_{p_B} \Bigg[& \frac{V_{\varepsilon_k \varepsilon_{k'} [o v'_B p_B]}}{\varepsilon_k + \varepsilon_{k'} - \varepsilon_{o v'_B} - \varepsilon_{p_B} + i0^+} \boldsymbol{D}_{p_B o v_B} \\
& - \frac{V_{\varepsilon_k \varepsilon_{k'} [o v_B p_B]}}{\varepsilon_k + \varepsilon_{k'} - \varepsilon_{o v_B} - \varepsilon_{p_B} + i0^+} \boldsymbol{D}_{p_B o v'_B} \Bigg] \\
& + \sum_{h_B} \Bigg[\boldsymbol{D}_{\varepsilon_k h_B} \frac{V_{h_B \varepsilon_{k'} [o v_B o v'_B]}}{\varepsilon_{h_B} + \varepsilon_{k'} - \varepsilon_{o v_B} - \varepsilon_{o v'_B}} \\
& - \boldsymbol{D}_{\varepsilon_{k'} h_B} \frac{V_{h_B \varepsilon_k [o v_B o v'_B]}}{\varepsilon_{h_B} + \varepsilon_k - \varepsilon_{o v_B} - \varepsilon_{o v'_B}} \Bigg] \\
& + \sum_{p_B} \Bigg[- \boldsymbol{D}_{\varepsilon_{k'} p_B} \frac{V_{p_B \varepsilon_k [o v_B o v'_B]}}{\varepsilon_{p_B} + \varepsilon_k - \varepsilon_{o v_B} - \varepsilon_{o v'_B}} \\
& + \boldsymbol{D}_{\varepsilon_k p_B} \frac{V_{p_B \varepsilon_{k'} [o v_B o v'_B]}}{\varepsilon_{p_B} + \varepsilon_{k'} - \varepsilon_{o v_B} - \varepsilon_{o v'_B}} \Bigg] \\
& + \sum_{h_B} \Bigg[- \frac{V_{\varepsilon_k \varepsilon_{k'} [o v_B h_B]}}{\varepsilon_k + \varepsilon_{k'} - \varepsilon_{o v_B} - \varepsilon_{h_B}} \boldsymbol{D}_{h_B o v'_B} \\
& + \frac{V_{\varepsilon_k \varepsilon_{k'} [o v'_B h_B]}}{\varepsilon_k + \varepsilon_{k'} - \varepsilon_{o v'_B} - \varepsilon_{h_B}} \boldsymbol{D}_{h_B o v_B} \Bigg]. \qquad \text{(C4)}
\end{aligned}
$$

The first two sums arise from the final-state expansions and can be identified as knock-out and shake-off mechanisms. The knock-out terms have singularities, because $\varepsilon_{p_B} = \varepsilon_k + \varepsilon_{k'} - \varepsilon_{o v_B}/\varepsilon_{o v'_B}$ and therefore, $+i0^+$ is inserted into the energy denominator. The last two sums come from the initial-state expansion and describe the ground-state correlations. Before the single-differential partial cross section $\frac{d\sigma_B^{++}(\omega)}{d\varepsilon_{k'}}$ is derived, one has to average over the initial-state degeneracies, which is omitted in the case of the nondegenerate ground state, and sum over the final-state degeneracies (see Appendix B).

[1] R. Dörner, H. Schmidt-Böcking, T. Weber, T. Jahnke, M. Schöffler, A. Knapp, M. Hattass, A. Czasch, L. Ph. H. Schmidt, and O. Jagutzki, Radiat. Phys. Chem. **70**, 191 (2004).

[2] T. N. Chang and R. T. Poe, Phys. Rev. A **12**, 1432 (1975).

[3] K.-i. Hino, T. Ishihara, F. Shimizu, N. Toshima, and J. H. McGuire, Phys. Rev. A **48**, 1271 (1993).

[4] C. Pan and H. P. Kelly, J. Phys. B: At. Mol. Opt. Phys. **28**, 5001 (1995).

[5] R. Wehlitz, P. N. Juranić, and D. V. Lukić, Phys. Rev. A **78**, 033428 (2008).

[6] M. Y. Amusia, I. S. Lee, and V. A. Kilin, Phys. Rev. A **45**, 4576 (1992).

[7] P. Kolorenč, V. Averbukh, R. Feifel, and J. Eland, J. Phys. B: At. Mol. Opt. Phys. **49**, 082001 (2016).

[8] F. Zhou, Y. Ma, and Y. Qu, Phys. Rev. A **93**, 060501(R) (2016).

[9] Y. Ma, F. Zhou, L. Liu, and Y. Qu, Phys. Rev. A **96**, 042504 (2017).

[10] J. Viefhaus, A. Grum-Grzhimailo, N. Kabachnik, and U. Becker, J. Electron Spectrosc. Relat. Phenom. **141**, 121 (2004).

[11] P. Berman, E. Arimondo, and C. Lin, *Advances in Atomic, Molecular, and Optical Physics* (Elsevier Science, London, UK, 2010), Vol. 58.

[12] R. Wehlitz, F. Heiser, O. Hemmers, B. Langer, A. Menzel, and U. Becker, Phys. Rev. Lett. **67**, 3764 (1991).

[13] T. Hartman, P. N. Juranić, K. Collins, B. Reilly, E. Makoutz, N. Appathurai, and R. Wehlitz, Phys. Rev. A **87**, 063403 (2013).

[14] A. S. Kheifets and I. Bray, Phys. Rev. A **75**, 042703 (2007).

[15] M. S. Pindzola, C. P. Ballance, S. A. Abdel-Naby, F. Robicheaux, G. S. J. Armstrong, and J. Colgan, J. Phys. B: At. Mol. Opt. Phys. **46**, 035201 (2013).

[16] F. L. Yip, T. N. Rescigno, and C. W. McCurdy, Phys. Rev. A **94**, 063414 (2016).

[17] J. Zeng, P. Liu, W. Xiang, and J. Yuan, Phys. Rev. A **87**, 033419 (2013).

[18] T. Hayaishi, E. Murakami, Y. Morioka, E. Shigemasa, A. Yagishita, and F. Koike, J. Phys. B: At. Mol. Opt. Phys. **28**, 1411 (1995).

[19] R. Wehlitz, J. Phys. B: At. Mol. Opt. Phys. **49**, 222004 (2016).

[20] V. Averbukh and L. S. Cederbaum, Phys. Rev. Lett. **96**, 053401 (2006).

[21] L. S. Cederbaum, J. Zobeley, and F. Tarantelli, Phys. Rev. Lett. **79**, 4778 (1997).

[22] V. Averbukh, P. Demekhin, P. Kolorenč, S. Scheit, S. Stoychev, A. Kuleff, Y.-C. Chiang, K. Gokhberg, S. Kopelke, N. Sisourat, and L. Cederbaum, J. Electron Spectrosc. Relat. Phenom. **183**, 36 (2011).

[23] U. Hergenhahn, J. Electron Spectrosc. Relat. Phenom. **184**, 78 (2011).

[24] T. Jahnke, J. Phys. B: At. Mol. Opt. Phys. **48**, 082001 (2015).

[25] T. Jahnke, U. Hergenhahn, B. Winter, R. Dörner, U. Frühling, P. V. Demekhin, K. Gokhberg, L. S. Cederbaum, A. Ehresmann, A. Knie, and A. Dreuw, Chem. Rev. **120**, 11295 (2020).

[26] V. Averbukh, I. B. Müller, and L. S. Cederbaum, Phys. Rev. Lett. **93**, 263002 (2004).

[27] K. Gokhberg, S. Kopelke, N. V. Kryzhevoi, P. Kolorenč, and L. S. Cederbaum, Phys. Rev. A **81**, 013417 (2010).

[28] C. Müller, M. A. Macovei, and A. B. Voitkiv, Phys. Rev. A **84**, 055401 (2011).

[29] J. L. Hemmerich, R. Bennett, and S. Y. Buhmann, Nat. Commun. **9**, 2934 (2018).

[30] A. C. LaForge, M. Shcherbinin, F. Stienkemeier, R. Richter, R. Moshammer, T. Pfeifer, and M. Mudrich, Nat. Phys. **15**, 247 (2019).

[31] A. Eckey, A. B. Voitkiv, and C. Müller, J. Phys. B: At. Mol. Opt. Phys. **53**, 055001 (2020).

[32] P. Kolorenč and V. Averbukh, J. Chem. Phys. **152**, 214107 (2020).

[33] S. Marburger, O. Kugeler, U. Hergenhahn, and T. Möller, Phys. Rev. Lett. **90**, 203401 (2003).

[34] G. Öhrwall, M. Tchaplyguine, M. Lundwall, R. Feifel, H. Bergersen, T. Rander, A. Lindblad, J. Schulz, S. Peredkov, S. Barth, S. Marburger, U. Hergenhahn, S. Svensson, and O. Björneholm, Phys. Rev. Lett. **93**, 173401 (2004).

[35] M. Mucke, M. Braune, S. Barth, M. Förstel, T. Lischke, V. Ulrich, T. Arion, U. Becker, A. Bradshaw, and U. Hergenhahn, Nat. Phys. **6**, 143 (2010).

[36] T. Jahnke, H. Sann, T. Havermeier, K. Kreidi, C. Stuck, M. Meckel, M. Schöffler, N. Neumann, R. Wallauer, S. Voss, A. Czasch, O. Jagutzki, A. Malakzadeh, F. Afaneh, T. Weber, H. Schmidt-Böcking, and R. Dörner, Nat. Phys. **6**, 139 (2010).

[37] V. Stumpf, K. Gokhberg, and L. S. Cederbaum, Nat. Chem. **8**, 237 (2016).

[38] F. Trinter, J. B. Williams, M. Weller, M. Waitz, M. Pitzer, J. Voigtsberger, C. Schober, G. Kastirke, C. Müller, C. Goihl, P. Burzynski, F. Wiegandt, R. Wallauer, A. Kalinin, L. P. H. Schmidt, M. S. Schöffler, Y.-C. Chiang, K. Gokhberg, T. Jahnke, and R. Dörner, Phys. Rev. Lett. **111**, 233004 (2013).

[39] A. I. Kuleff, K. Gokhberg, S. Kopelke, and L. S. Cederbaum, Phys. Rev. Lett. **105**, 043004 (2010).

[40] F. Trinter, M. S. Schöffler, H.-K. Kim, F. P. Sturm, K. Cole, N. Neumann, A. Vredenborg, J. Williams, I. Bocharova, R. Guillemin, M. Simon, A. Belkacem, A. L. Landers, T. Weber, H. Schmidt-Böcking, R. Dörner, and T. Jahnke, Nature (London) **505**, 664 (2014).

[41] K. Gokhberg, P. Kolorenč, A. I. Kuleff, and L. S. Cederbaum, Nature (London) **505**, 661 (2014).

[42] I. I. Sobel'man, *Introduction to the Theory of Atomic Spectra*, International Series of Monographs in Natural Philosophy (Pergamon Press, Oxford, UK, 1972).

[43] L. S. Cederbaum, Phys. Rev. Lett. **121**, 223001 (2018).

[44] F. Mertins, Studien zur photoionisierung und vielteilchentheorie von molekülen, Ph.D. thesis, Ruprecht-Karls-Universität Heidelberg, 1995.

[45] J. C. Tully, R. S. Berry, and B. J. Dalton, Phys. Rev. **176**, 95 (1968).

[46] I. Shavitt and R. Bartlett, *Many-Body Methods in Chemistry and Physics: MBPT and Coupled-Cluster Theory*, Cambridge Molecular Science (Cambridge University Press, Cambridge, UK, 2009).

[47] U. Fano, Phys. Rev. **124**, 1866 (1961).

[48] J. Zobeley, R. Santra, and L. S. Cederbaum, J. Chem. Phys. **115**, 5076 (2001).

[49] M.-S. Son and Y. Kiel Sung, Chem. Phys. Lett. **245**, 113 (1995).

[50] V. Srdanov, A. Saab, D. Margolese, E. Poolman, K. Khemani, A. Koch, F. Wudl, B. Kirtman, and G. Stucky, Chem. Phys. Lett. **192**, 243 (1992).

[51] M. C. Böhm, T. Schedel-Niedrig, H. Werner, R. Schlögl, J. Schulte, and J. Schütt, Z. Naturforsch. A **51**, 283 (1996).

[52] National Institute of Standards and Technology Atomic Spectra Database, https://www.nist.gov/pml/atomic-spectra-database.

[53] P. N. Juranić, D. Lukić, K. Barger, and R. Wehlitz, Phys. Rev. A **73**, 042701 (2006).

[54] R. Wehlitz, private communication (2019).

[55] A. Reinköster, S. Korica, G. Prümper, J. Viefhaus, K. Godehusen, O. Schwarzkopf, M. Mast, and U. Becker, J. Phys. B: At. Mol. Opt. Phys. **37**, 2135 (2004).

[56] A. Lyras and H. Bachau, J. Phys. B: At. Mol. Opt. Phys. **38**, 1119 (2005).

[57] B. Karaçoban Usta, Can. J. Phys. **97**, 828 (2019).

[58] A. M. Weigold and J. A. Piper, Opt. Lett. **15**, 1209 (1990).

[59] V. Pejcev, T. W. Ottley, D. Rassi, and K. J. Ross, J. Phys. B: At. Mol. Opt. Phys. **10**, 2389 (1977).

[60] R. Wehlitz, J. Colgan, M. Martinez, J. Bluett, D. Lukić, and S. Whitfield, J. Electron Spectrosc. Relat. Phenom. **144-147**, 59 (2005).

[61] P. N. Juranić, J. Nordberg, and R. Wehlitz, Phys. Rev. A **74**, 042707 (2006).

[62] B. Rouvellou, L. Journel, J. M. Bizau, D. Cubaynes, F. J. Wuilleumier, M. Richter, K.-H. Selbmann, P. Sladeczek, and P. Zimmermann, Phys. Rev. A **50**, 4868 (1994).

[63] J. A. R. Samson, W. C. Stolte, Z.-X. He, J. N. Cutler, Y. Lu, and R. J. Bartlett, Phys. Rev. A **57**, 1906 (1998).

[64] R. Wehlitz, I. A. Sellin, O. Hemmers, S. B. Whitfield, P. Glans, H. Wang, D. W. Lindle, B. Langer, N. Berrah, J. Viefhaus, and U. Becker, J. Phys. B: At. Mol. Opt. Phys. **30**, L51 (1997).

[65] R. Dörner, T. Vogt, V. Mergel, H. Khemliche, S. Kravis, C. L. Cocke, J. Ullrich, M. Unverzagt, L. Spielberger, M. Damrau, O. Jagutzki, I. Ali, B. Weaver, K. Ullmann, C. C. Hsu, M. Jung, E. P. Kanter, B. Sonntag, M. H. Prior, E. Rotenberg, J. Denlinger, T. Warwick, S. T. Manson, and H. Schmidt-Böcking, Phys. Rev. Lett. **76**, 2654 (1996).

[66] A. S. Kheifets and I. Bray, Phys. Rev. A **58**, 4501 (1998).

[67] A. Kheifets, private communication (2019).

[68] J. Bouwman, P. Castellanos, M. Bulak, J. Terwisscha van Scheltinga, J. Cami, H. Linnartz, and A. G. G. M. Tielens, Astron. Astrophys. **621**, A80 (2019).

[69] D. K. Bohme, Chem. Rev. **92**, 1487 (1992).

[70] Y. Xie and L. C. Ho, Astrophys. J. **884**, 136 (2019).

[71] D. C. Griffin, D. M. Mitnik, and N. R. Badnell, J. Phys. B: At. Mol. Opt. Phys. **34**, 4401 (2001).

[72] A. Picón, C. Buth, G. Doumy, B. Krässig, L. Young, and S. H. Southworth, Phys. Rev. A **87**, 013432 (2013).

[73] N. Rohringer and R. Santra, Phys. Rev. A **77**, 053404 (2008).

[74] M. Coreno, L. Avaldi, R. Camilloni, K. C. Prince, M. de Simone, J. Karvonen, R. Colle, and S. Simonucci, Phys. Rev. A **59**, 2494 (1999).

[75] M. Bartolomei, E. Carmona-Novillo, M. I. Hernández, J. Campos-Martínez, and F. Pirani, J. Phys. Chem. C **117**, 10512 (2013).

[76] O. Stauffert, S. Izadnia, F. Stienkemeier, and M. Walter, J. Chem. Phys. **150**, 244703 (2019).

[77] T. Brupbacher, H. Lüthi, and A. Bauder, Chem. Phys. Lett. **195**, 482 (1992).

[78] A. Hans, C. Küstner-Wetekam, P. Schmidt, C. Ozga, X. Holzapfel, H. Otto, C. Zindel, C. Richter, L. S. Cederbaum, A. Ehresmann, U. Hergenhahn, N. V. Kryzhevoi, and A. Knie, Phys. Rev. Res. **2**, 012022(R) (2020).

[79] N. Sisourat, N. V. Kryzhevoi, P. Kolorenč, S. Scheit, T. Jahnke, and L. S. Cederbaum, Nat. Phys. **6**, 508 (2010).

[80] T. Havermeier, T. Jahnke, K. Kreidi, R. Wallauer, S. Voss, M. Schöffler, S. Schössler, L. Foucar, N. Neumann, J. Titze, H. Sann, M. Kühnel, J. Voigtsberger, J. H. Morilla, W. Schöllkopf, H. Schmidt-Böcking, R. E. Grisenti, and R. Dörner, Phys. Rev. Lett. **104**, 133401 (2010).

[81] L. Liu, P. Kolorenč, and K. Gokhberg, Phys. Rev. A **101**, 033402 (2020).
[82] W. Pokapanich, N. V. Kryzhevoi, N. Ottosson, S. Svensson, L. S. Cederbaum, G. Öhrwall, and O. Björneholm, J. Am. Chem. Soc. **133**, 13430 (2011).
[83] R. Santra, J. Zobeley, and L. S. Cederbaum, Phys. Rev. B **64**, 245104 (2001).
[84] N. V. Kryzhevoi, V. Averbukh, and L. S. Cederbaum, Phys. Rev. B **76**, 094513 (2007).
[85] V. Stumpf, C. Brunken, and K. Gokhberg, J. Chem. Phys. **145**, 104306 (2016).
[86] R. P. Madden and K. Codling, Phys. Rev. Lett. **10**, 516 (1963).
[87] J. M. Rost, K. Schulz, M. Domke, and G. Kaindl, J. Phys. B: At. Mol. Opt. Phys. **30**, 4663 (1997).
[88] G. Jabbari, K. Gokhberg, and L. S. Cederbaum, Chem. Phys. Lett. **754**, 137571 (2020).
[89] V. Averbukh and L. S. Cederbaum, J. Chem. Phys. **123**, 204107 (2005).
[90] V. Averbukh and L. S. Cederbaum, J. Chem. Phys. **125**, 094107 (2006).
[91] P. Kolorenč, N. V. Kryzhevoi, N. Sisourat, and L. S. Cederbaum, Phys. Rev. A **82**, 013422 (2010).
[92] S. Kopelke, K. Gokhberg, V. Averbukh, F. Tarantelli, and L. S. Cederbaum, J. Chem. Phys. **134**, 094107 (2011).
[93] A. Y. Istomin, N. L. Manakov, and A. F. Starace, J. Phys. B: At. Mol. Opt. Phys. **35**, L543 (2002).
[94] S. P. Lucey, J. Rasch, C. T. Whelan, and H. R. J. Walters, J. Phys. B: At. Mol. Opt. Phys. **31**, 1237 (1998).
[95] F. Maulbetsch and J. S. Briggs, J. Phys. B: At. Mol. Opt. Phys. **27**, 4095 (1994).
[96] A. Szabo and N. Ostlund, *Modern Quantum Chemistry: Introduction to Advanced Electronic Structure Theory*, Dover Books on Chemistry (Dover Publications, Inc., Mineola, New York, 2012).
[97] J. Schirmer, *Many-Body Methods for Atoms, Molecules and Clusters*, Lecture Notes in Chemistry (Springer International Publishing, Cham, Switzerland, 2018).